Chemical Science

ROYAL SOCIETY OF CHEMISTRY

REVIEW

View Article Online
View Journal | View Issue

Cite this: *Chem. Sci.*, 2024, **15**, 9927

Recent advances in CO_2 reduction with renewable reductants under hydrothermal conditions: towards efficient and net carbon benefit CO_2 conversion

Zien Tang,[a] Xu Liu,[a] Yang Yang*[a] and Fangming Jin *[abc]

The ever-growing atmospheric CO_2 concentration threatening the environmental sustainability of humankind makes the reduction of CO_2 to chemicals or fuels an ideal solution. Two priorities are anticipated for the conversion technology, high efficiency and net carbon benefit, to ensure the mitigation of the CO_2 problem both promptly and sustainably. Until now, catalytic hydrogenation or solar/electro-chemical CO_2 conversion have achieved CO_2 reduction promisingly while, to some extent, compromising to fulfill the two rules, and thus alternative approaches for CO_2 reduction are necessary. Natural geochemical processes as abiotic CO_2 reductions give hints for efficient CO_2 reduction by building hydrothermal reaction systems, and this type of reaction atmosphere provides room for introducing renewable substances as reductants, which offers the possibility to achieve CO_2 reduction with net carbon benefit. While the progress in CO_2 reduction has been abundantly summarized, reviews on hydrothermal CO_2 reduction are relatively scarce and, more importantly, few have focused on CO_2 reduction with renewable reductants with the consideration of both scale of efficiency and sustainability. This review provides a fundamental and critical review of metal, biomass and polymer waste as reducing agents for hydrothermal CO_2 reduction. Various products including formic acid, methanol, methane and multi-carbon chemicals can be formed, and effects of operational parameters such as temperature, batch holding time, pH value and water filing as well as detailed reaction mechanisms are illustrated. Particularly, the critical roles of high temperature and pressure water as reaction promotor and catalyst in hydrothermal CO_2 conversion are discussed at the mechanistic level. More importantly, this review compares hydrothermal CO_2 reduction with other methods such as catalytic hydrogenation and photo/

Received 22nd February 2024
Accepted 19th May 2024

DOI: 10.1039/d4sc01265h

rsc.li/chemical-science

[a]*School of Environmental Science and Engineering, State Key Laboratory of Metal Matrix Composites, Shanghai Jiao Tong University, Shanghai 200240, P. R. China. E-mail: fmjin@sjtu.edu.cn; yangyang0120@sjtu.edu.cn*

[b]*Shanghai Key Laboratory of Hydrogen Science, Center of Hydrogen Science, Shanghai Jiao Tong University, Shanghai 200240, P. R. China*

[c]*Shanghai Institute of Pollution Control and Ecological Security, Shanghai 200092, P. R. China*

Zien Tang

Zien Tang received his master's degree in 2024 from the School of Environmental Science and Engineering at Shanghai Jiao Tong University, under the guidance of Professor Fangming Jin. His research interests focus on the hydrothermal co-conversion of lignin and CO_2.

Xu Liu

Xu Liu is a doctoral candidate at the School of Environmental Science and Engineering, Shanghai Jiao Tong University under the supervision of Prof. Fangming Jin. His research focuses on cobalt based catalytic CO_2 reduction under hydrothermal conditions and the corresponding density functional theory (DFT) calculations.

electrocatalysis, evaluating their efficiency and potential for net carbon benefit. The aim of this review is to promote the understanding of CO_2 activation under a hydrothermal environment and provide insights into the efficient and sustainable strategy of hydrothermal CO_2 conversion for future fundamental research and industrial applications.

1 Introduction

The world is currently facing an energy crisis since the demand for energy continuously grows to support the rapid development of the society. This has resulted in a heavy reliance on carbon-intensive energy sources, leading to increasing levels of carbon dioxide (CO_2) emissions. Given that CO_2 is a major greenhouse gas, extensive emissions of CO_2 will bring a series of negative impacts including global warming, ocean acidification, melting of polar ice caps, and other environmental problems.[1–3] As the world grapples with challenges related to climate change and energy security, the importance of utilizing CO_2 as a carbon resource is increasingly recognized for its potential to mitigate climate change and promote sustainable development. In this context, CO_2 can be viewed as a valuable resource that can be utilized in various ways such as in the production of fuels, chemicals, and materials,[4,5] which can reduce greenhouse gas emissions, create economic opportunities, and promote the transition to a low-carbon economy.

When fully considering the utilization of CO_2 as a carbon source to build an environmentally benign and sustainable society for the future, the underlying technologies are expected to achieve two targets: net carbon benefit and high efficiency, which ideally require no extra fossil fuel sourced energy during the whole CO_2 reduction process and simultaneously an efficient conversion process. This consideration aligns with the growing consensus that sustainability should be integrated into the performance metrics of conversion systems.[6] In recent years, various catalytic methods, including catalytic hydrogenation,[7,8] photo-catalysis,[9,10] electrocatalysis,[11,12] the recently arisen photo-thermal catalysis,[13,14] and photo-electro catalysis,[15,16] have been applied to convert CO_2 into high-value-added products. During these processes, carbon-containing compounds like formic acid, methanol, methane, acetic acid, ethylene, and even long-chain alkanes are formed, which can serve as chemical stocks or fuels depending on the circumstances.[17–19] However, bottlenecks in enhancing the efficiency of photo-catalysis or large consumption of high-quality electricity during the electro-catalytic CO_2 reduction process and the necessity of delicately prepared catalysts restrict their applications. For catalytic CO_2 hydrogenation, hydrogen is an essential raw material, yet it has complex systematic issues in its preparation, storage, and transportation processes, which rely heavily on fossil fuels as the energy supplier.[20] Consequently, to meet the undeniable requirements of net carbon benefit and highly efficient CO_2 reduction, alternative approaches that balance the paradox are anticipated.

Natural geochemical processes that regulate the carbon cycle, including the transformation of CO_2 over geological timescales, could be instrumental in counteracting anthropogenic CO_2 emissions. In the absence of solar irradiation and electrical power, Earth's natural hydrothermal reduction environments, enhanced by the significant catalytic properties of bedrock minerals, can abiotically reduce CO_2 into long-chain hydrocarbons and organic compounds like carboxylic acids.[21] This process is also postulated to have facilitated the origin of life and the formation of most natural petroleum deposits.[22,23] Mimicking this natural phenomenon, efficient CO_2 reduction could be achieved using artificially constructed hydrothermal reaction systems.[24] Compared to solar/electro-catalytic CO_2 reduction or catalytic CO_2 hydrogenation, under hydrothermal conditions, high-temperature water creates an environment

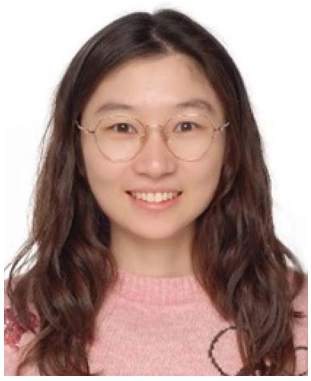

Yang Yang

Yang Yang obtained her PhD in 2019 from Shanghai Jiao Tong University, China, under the guidance of Prof. Fangming Jin. She is currently an Assistant Researcher at the School of Environmental Science and Engineering at Shanghai Jiao Tong University. Previously, she was a postdoctoral fellow in the same group (2019–2023) and was supported by the Postdoctoral Innovation Talents Support Program. Her research focuses on the conversion of CO_2 and biomass under hydrothermal conditions, aiming to develop sustainable and efficient technologies for CO_2 reduction.

Fangming Jin

Fangming Jin received her PhD in Earth Engineering from Tohoku University in 1999. She was a postdoctoral fellow and later an Assistant Professor and Associate Professor at Tohoku University until 2007. She became a Professor at Tongji University in 2007 and was honored as a Changjiang Scholars Program Distinguished Professor. Since 2011, she has been a Distinguished Professor at the School of Environmental Science and Engineering, Shanghai Jiao Tong University. Her research focuses on mimicking the natural hydrothermal environment for highly efficient conversion of biomass/waste and CO_2 to amend the carbon cycle.

that facilitates the utilization of various hydrogen sources, such as metals, biomass, and even organic waste, for CO_2 reduction, demonstrating a flexibility in selecting reductant feedstock which eliminates the need for gaseous hydrogen or high-quality electricity. Additionally, owing to the vigorousness of the hydrothermal reaction, highly efficient and fast CO_2 reduction could be achieved, providing prospects for large scale application. Further advances in hydrothermal CO_2 reduction lie in the direct reduction of bicarbonate or carbonate (HCO_3^- or CO_3^{2-}), since CO_2 generally needs to be captured from either the atmosphere or point sources by alkaline absorbents before utilization, and this process transforms CO_2 into HCO_3^- and/or CO_3^{2-} (the final products are pH dependent), while for solar/electro-catalytic CO_2 reduction or catalytic CO_2 hydrogenation, generally only gaseous CO_2 can be directly reduced. However, central to this geochemically inspired approach is the selection of appropriate reductants. The ideal reductants should be renewable hydrogen sources or regenerable through renewable energy, ensuring that the CO_2 reduction process aligns with the principles of sustainability.

A series of pioneering studies on CO_2 reduction by building hydrothermal reaction systems have been reported, in which various zero-valent metals such as Fe, Zn, Mn have been used as reductants for *in situ* hydrogen production.[25–51] While CO_2 was successfully reduced to C_1 or C_{2+} products, the zero-valent metals were oxidized to the corresponding metal oxides, leading to the metals being discarded after one use. To cope with this issue, the regeneration of metals using renewable energy becomes necessary. When Fe was used as the reductant to hydrothermally convert CO_2, the corresponding oxidized high valence metal could be reduced to zero valence by biomass or biomass derivatives with the formation of organic acids, which means no metal consumption during those processes, and both CO_2 and the biomass can be converted to high value-added products.[48,51–55] Furthermore, in the systematic work by A. Steinfeld,[56] the heat obtained from concentrated solar radiation was utilized to drive multiple cycles of metal oxide redox pairs, including Zn/ZnO, potentially offering Zn as another reductant for CO_2 conversion. This research substantiates the proposal that the reduction of CO_2 can be driven by the redox reactions of zero-valent metals (Fe or Zn), underscoring a critical mechanism by which these metals facilitate the transformation of CO_2 into various reduced forms without being consumed.

Intriguingly, biomass and bio-related organic compounds containing highly active and reductive functional groups (–OH, –CHO, $–NH_2$) can produce hydrogen in hydrothermal environments, rendering biochemicals as a viable hydrogen donor for CO_2 reduction. Since biomass stores solar energy, using it to drive CO_2 reduction offers great potential in achieving net-zero emission reaction systems. Moreover, as CO_2 is naturally fixed through photosynthesis in biomass, additional CO_2 reduction with biomass allows double CO_2 fixation. Following this concept, wastes such as polyvinyl chloride (PVC) have the potential to generate reductive functional groups such as –OH if processed properly, offering another potential and economic reductant for CO_2 reduction. Thus, the employment of regenerable metals, biomass, or organic waste as renewable reductants for CO_2 reduction under hydrothermal conditions becomes a plausible solution for efficient and net carbon benefit CO_2 reduction (the notion of CO_2 reduction with renewable reductants under hydrothermal conditions is illustrated in Fig. 1).

Despite the technologies for CO_2 reduction being readily summarized, hydrothermal CO_2 reduction is relatively new with scarce reviews in this field, and more importantly, few discuss this issue with consideration for both efficiency and sustainability. Starting with the advantages and geologic origin of a hydrothermal environment for CO_2 reduction, this minireview systematically summarizes recent advances in hydrothermal CO_2 reduction using metals (Fe or Zn), biomass, and polymer wastes, discussing operational factors such as temperature, reaction time, pH value, and pressure. The superiority of CO_2 reduction under hydrothermal conditions is illustrated at a mechanistic level, revealing the catalytic influence of hydrothermal conditions based on the intrinsic characteristics of the hydrothermal environment, with a specific section emphasizing the promoting function of water molecules. For the primary purpose of advancing CO_2 reduction with net carbon benefit and high efficiency, this review compares the summarized approaches with reported methods such as catalytic hydrogenation or photo/electric catalyzed CO_2 reduction, analyzing the degree of carbon mitigation, and therefore provides insights on the efficient and sustainable strategy of hydrothermal CO_2 conversion for future fundamental research and industrial applications.

2 The origin of life under hydrothermal conditions and insights on CO_2 reduction

High temperature and high pressure water (HTHP water) in hydrothermal conditions is recognized as an important factor in various geological processes, such as hydrothermal circulation, ore deposition, and rock alteration,[57] occurring in both

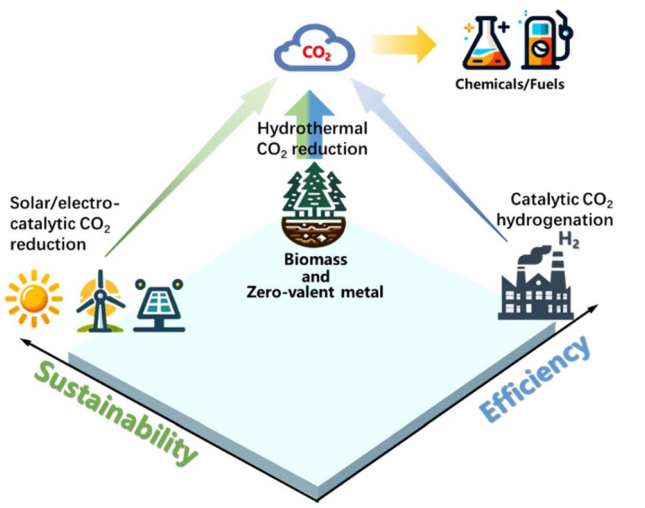

Fig. 1 Comparison of CO_2 reduction by renewable reductants under hydrothermal conditions with solar/electro-catalytic CO_2 reduction or catalytic CO_2 hydrogenation.

sub-aerial and sub-seafloor environments and profoundly affecting the physicochemical properties of rocks and fluids. At elevated temperature and pressure, HTHP water exhibits as good solubility for organics and gases as many nonpolar organic solvents due to its lower dielectric constant (ε), which decreases from about 80 at ambient condition to 5 at the critical point[58–60] (374 °C and 22.1 MPa). Another significant factor is the ionic product of HTHP water ($K_w = [H^+]\cdot[OH^-]$; $[H^+] = [OH^-]$). For instance, at ambient conditions, K_w is 10^{-14} (mol kg^{-1}),[2] but it can sharply rise to a maximum of 10^{-11} at around 250 °C.[61] This increase in the concentration of H^+ or OH^- ions can facilitate acid/base-catalyzed reactions, which can significantly accelerate reactions, such as the dehydration of carbohydrates and alcohols. The diffusion rate of supercritical water is reduced to nearly 1/100 that of liquid water. The weak interaction of hydrogen bonds among water molecules in the HTHP water phase eliminates the mass transfer resistance between interfaces.[62] Consequently, the efficient heat transfer and rapid mass diffusion resulting from the high diffusion rate and low viscosity of HTHP water promote reaction rates, hopefully contributing to invoke the reductive capacity of metals or organic hydrogen sources for CO_2 reduction.[59,63]

Due to its unique properties, HTHP water has been proposed as a possible setting for the origin of life on Earth. Hydrothermal vents are fissures in the Earth's surface, often found along mid-ocean ridges, where superheated water, gases (CH_4, CO_2, H_2S and H_2), minerals (pyrrhotite, sphalerite, pyrite and copper-iron sulfide) and metals (mainly Fe, Co and Mg) are expelled from the ocean floor.[64] The presence of those mineral surfaces in hydrothermal environments enhances the stability and reactivity of organic compounds and provides catalytic surfaces for prebiotic reactions.[65] Furthermore, the hydrothermal environment can protect organic molecules from destructive radiation and other environmental stresses, providing a dynamic and energy-rich environment for the emergence and evolution of early life forms.[66]

Inspired by the theory of the origin of deep-sea life, a series of studies on CO_2 conversion under hydrothermal conditions was conducted. Fiebig *et al.*[67] provided definitive evidence that CH_4 is generated from mixed aliquots of limestone and mantle-derived CO_2 in volcanic hydrothermal systems. It was found that CH_4 generation highly depends on the availabilities of Fe^{2+}, CO_2 and H_2O and on reaction kinetics. Furthermore, He *et al.* demonstrated that the formation of Fe–OH during hydrothermal CO_2 processing can enhance the adsorption of the siderite-derived CO intermediate on Co, facilitating efficient C–C coupling in which C_{24+} long chain hydrocarbons were synthesized under 300 °C and 30 MPa hydrothermal conditions.[25] These findings support the abiogenic hypothesis for petroleum deposits, propose a method for nonnoble metal-catalyzed CO_2 conversion to petroleum fuel, and contribute to a better understanding of the emergence of life. Amino acids, such as glycine, can also be synthesized from simple inorganic chemicals like HCHO and NH_3,[68] which suggests the huge potential of the hydrothermal environment for CO_2 reduction.

Considering the unique characteristics of HTHP water, the influence of hydrothermal conditions on CO_2 conversion can be summarized as follows: (1) temperature and reaction time. Temperature directly affects the ion product and dielectric constant of high-temperature water (HTW). At 350 °C, hydrothermal products like formic acid primarily decompose into H_2 and CH_4.[69] This finding underscores the importance of selecting appropriate temperature and time ranges for reducing CO_2. Furthermore, different reductants such as metals or biomass require different reaction temperatures to stimulate hydrogen production. For most metal-based reactions, the ideal temperature and reaction time are around 250 °C and 2 h, respectively. Biomass, however, requires a higher temperature of 300 °C or a longer time of 3 h, probably owing to the lower reducing capacity of biomass-derived functional groups compared to metal compounds. (2) Water filling and pressure. Water filling affects the reaction pressure, which significantly impacts CO_2 dissolution and hydrogen partial pressure. Higher pressure promotes higher reduction efficiency by enhancing CO_2 activation and facilitating the reaction direction *via* H_2 consumption.[30] (3) Solution pH and concentration of CO_2, HCO_3^- or CO_3^{2-}. Solution pH affects CO_2 reduction because an acid or alkaline environment can convert CO_2 to HCO_3^- or CO_3^{2-}, and different carbon sources lead to different products such as methanol, methane, formic acid and multi-carbon products. Furthermore, a volcano-type relationship generally exists between the carbon source concentration and product yields, with a proper carbon source concentration favoring reduction efficiency while decreasing or increasing the concentration inhibits efficient reduction.

When applying hydrothermal technology for CO_2 reduction at lab scale, autoclave reactors, which can be heated to 200–400 °C and hold pressure from 1 atm to 300 atm, are generally adopted. According to their different heating systems, three sets of apparatus are used, such as (1) six-batch autoclaves and Parr reactors, which are heated through resistance wire; (2) SUS 316 tubular reactors, which are used in a salt bath and (3) electromagnetic induction reactors heated by the electromagnetic effect (Fig. 2). Due to the different heating rates and stirring modes provided by the different apparatus, each reactor is

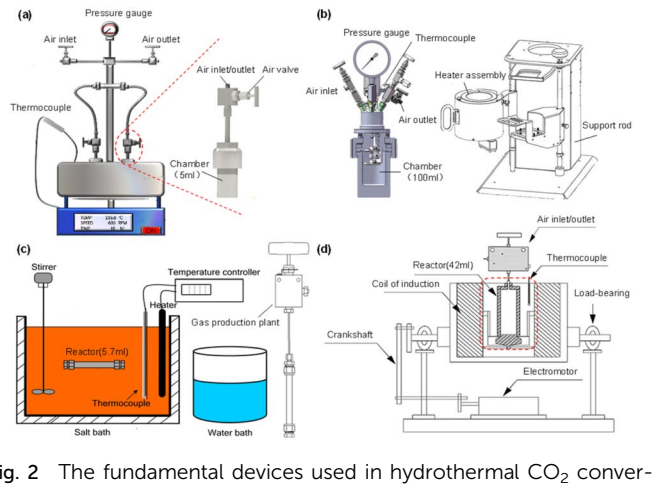

Fig. 2 The fundamental devices used in hydrothermal CO_2 conversion. (a) Six-batch autoclaves, (b) Parr reactor, (c) SUS 316 tubular reactor, (d) electromagnetic induction reactor.

applied in different scenarios. For instance, six-batch autoclaves and Parr reactors are the most used reactors, as the Parr reactor offers a larger capacity, allowing exploration of industrial-scale processes with real-time monitoring of temperature and pressure. On the other hand, when rapid heating rates are needed, SUS 316 tubular reactors are used; they are commonly chosen when biomass serves as the reductant. The electromagnetic induction reactor has a larger volume and, under the influence of a magnetic field, effective CO_2 reduction to long-chain hydrocarbons or multi-carbon products is achieved.

3 Hydrothermal CO_2 reduction with zero-valent metal/metal oxide redox cycles

The strategy for CO_2 reduction under hydrothermal conditions using zero-valent metal (M^0)/metal oxide (MO_x) redox cycles involves the production of formic acid and hydrogen *via* the oxidation of the M^0 in the first step. In the second step, MO_x is reduced with solar energy or by a suitable biomass derivative such as glycerin or glucose, resulting in the production of organic acids like formic, acetic, and lactic acids, as shown in Fig. 3. In this context, the following section summarizes CO_2 hydrothermal reduction with Fe or Zn as the reductant, focusing on the reaction characteristics, parameters, and mechanism.

3.1 Hydrothermal CO_2 reduction with Fe

Using Fe powder as the reductant in a hydrothermal environment, Nakamichi Yamasaki commenced CO_2 reduction at the beginning of this century.[70] He developed a continuous flow system operating at 200 °C and 2.0 MPa of constant CO_2 flow in a hydrothermal environment. When processing carbon steel scraps without Ni powder, no organic compounds were detected. However, with the addition of Ni powder, formic acid formation was observed. Extending the reaction time to 72 hours, He *et al.*[53] used Fe powder as a reductant at 200 °C to successfully reduce CO_2 to formic and acetic acids. During this process, Fe powder acts both as a reductant and a catalyst for CO_2 reduction. As illustrated in Fig. 4a, the reaction begins with Fe powder reacting with water to generate H_2, while dissolved CO_2 molecules are adsorbed on the surface of Fe. Under the influence of hydrogen, CO_2 is reduced to intermediate A, which subsequently hydrolyzes to form formic acid. Intermediate A continues to react with hydrogen, forming intermediate B, and, eventually, intermediates A and B react to form intermediate C, hydrolyzing into acetic acid. Additionally, phenol can be formed with Fe powder at 200 °C, 1.4 MPa CO_2, and 120 h of hydrothermal conditions with a yield of 1.21%.[71] The reaction mechanism, shown in Fig. 4b, involves CO_2 adsorption and binding to the Fe surface. Concurrently, Fe reacts with water to produce H_2 and Fe^{2+}. On the Fe powder surface, activated CO_2 forms formaldehyde, eventually transforming into phenol under the action of hydrogen. This process includes two simple reaction types: oxidative coupling and rearrangement reactions. The generation of H_2 is the rate-determining step in accelerating the reaction, and water is essential as a hydrogen source. Once hydrogen is produced from the reaction of Fe with water, the reaction proceeds rapidly, and the yield of phenol increases in acidic media.[72] Wu *et al.*[55] initially utilized $NaHCO_3$ to replace CO_2 in the reaction, due to the fact that, under high-temperature and high-pressure conditions, CO_2 readily dissolves in alkaline aqueous solutions, which leads to an equilibrium involving CO_2, H_2O, HCO_3^-, CO_3^{2-}, and OH^- ions, similar to conditions in $NaHCO_3$ aqueous solutions. No hydrogen was generated in the absence of $NaHCO_3$, while the hydrogen yield linearly increased with the addition of $NaHCO_3$, indicating that $NaHCO_3$ can effectively enhance hydrogen production from HTHP water. XRD and Raman results indicated no change in Fe valence in the absence of $NaHCO_3$; however, Fe was oxidized to Fe_3O_4 in the presence of $NaHCO_3$, accompanied by the formation of hydrogen gas. Furthermore, with an increase in $NaHCO_3$ concentration, an increase in Fe_3O_4 crystallization was observed. Thus, hydrogen was produced from the reaction of H_2O with Fe enhanced by $NaHCO_3$. For formate yield from hydrothermal $NaHCO_3$ conversion, the amount of Fe significantly influenced the yield. The formate yield increased from 1.6% to 10.7% when raising the Fe amount from 2 to 8 mmol under the conditions of 1 mmol $NaHCO_3$, 2 mL H_2O, 573 K, 2 h time and 35% water filling.

To enhance the productivity of CO_2 reduction with Fe under hydrothermal conditions for possible application of the reaction, heterogeneous catalysts were added. The impact of Ni addition was demonstrated, and the yield of formic acid increased from 1.16% to 5.4% with incorporation of Ni.[55] The Ni/Fe ratio significantly influences the yield of formic acid. As the Ni/Fe ratio increased from 1/2 to 1/1, the yield of formic acid rose from 9.1% to 15.6%. However, a higher Ni/Fe ratio resulted in a slight decrease in yield, as more Ni sites facilitated the conversion of formic acid to CH_4. Additionally, Chen *et al.*[69] found that temperatures exceeding 350 °C, particularly under supercritical water conditions, significantly accelerated the further reduction of formic acid to methane. Like Ni, Cu exhibited both positive and negative effects on formic acid formation. With Cu additions of less than 12 mmol, there was an increase in the yield of formic acid. However, when Cu exceeded 12 mmol, a sharp decrease in the yield of formic acid occurred, as excessive Cu led to the decomposition of formic acid. The highest formic acid yield, 71.3%, was achieved under the conditions of Fe : Cu = 1 : 1 for 2 h at 573 K.[48] In summary,

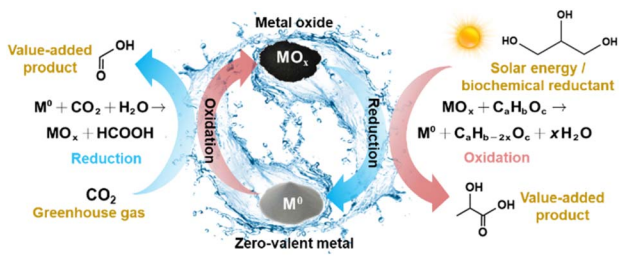

Fig. 3 Hydrothermal CO_2 reduction with zero-valent metal/metal oxide redox cycles.

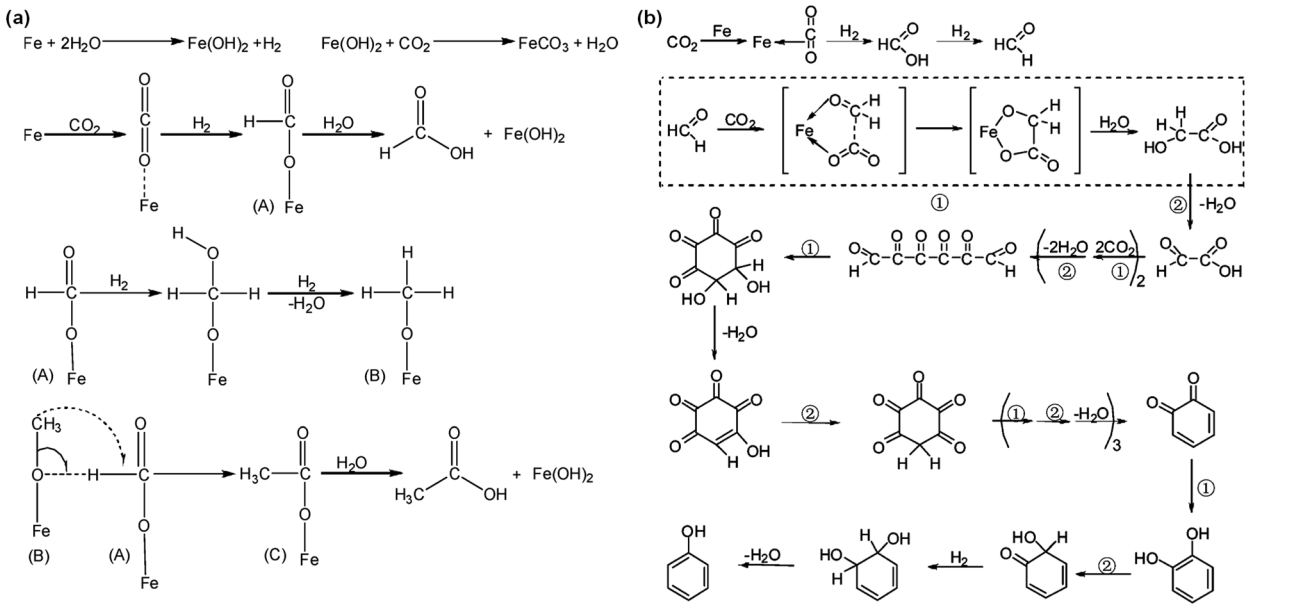

Fig. 4 (a) Proposed mechanism for the formation of formic acid and acetic acid in the presence of Fe powder and CO_2 under hydrothermal conditions.[53] This figure has been reproduced from ref. 53 with permission from American Chemical Society, copyright 2010. (b) Proposed mechanism of phenol formation[72] (① refers to the oxidative coupling reactions, and ② refers to the rearrangement reactions). This figure has been reproduced from ref. 72 with permission from American Chemical Society, copyright 2007.

with Ni or Cu as the catalyst, an appropriate amount is essential to maximize the yield of formic acid.

A significant breakthrough in CO_2 hydrothermal reduction using Fe as the reductant occurred upon proper adjustment of the Fe amount. Duo *et al.*[52] found that the amount of Fe was a decisive factor for CO_2 reduction. Under the conditions of 1 mmol per L $NaHCO_3$, 300 °C and 2 h, formate yield was dramatically increased from 12% to a peak of 91% as Fe loading was increased from 4 mmol to 24 mmol. Integrating XRD, XPS characterization analysis, and kinetic experimental results, a self-catalytic reaction mechanism was proposed, incorporating a short induction and a rapid formation phase. Initially, in the first 5–10 minutes, hydrogen and Fe_3O_4 with more oxygen vacancies (Fe_3O_{4-x}) were formed. Subsequently, this oxygen vacancy containing Fe_3O_{4-x} served as a catalyst to convert HCO_3^-, leading to a sharp increase in formate yield during the 10-30 minute period. Kinetic modelling indicates that the activation energy for the formate formation from HCO_3^- reduction is 28 kJ mol^{-1},[74] much lower than the 80 kJ mol^{-1} reported in previous studies on conventional hydrogenation of CO_2 using pincer-supported Ni hydrides as a catalyst,[75] demonstrating the supportive contribution of the self-catalytic reaction mechanism. Further support for the self-catalytic mechanism was obtained from the XPS analysis for both recovered and commercially available Fe_3O_4. As shown in Fig. 5a, the Fe^{2+}/Fe^{3+} ratio of the recovered Fe_3O_4 was 0.89 : 0.11, which is higher than the theoretical ratio of Fe_3O_4 (0.33 : 0.67), indicating *in situ* reduction of Fe^{3+} into Fe^{2+} on the surface of Fe_3O_4. This result was likely caused by the hydrogen formation from Fe oxidation, enhanced by the presence of $NaHCO_3$.

Based on the experimental results, a possible mechanism for the reduction of $NaHCO_3$ to formate by Fe is proposed in Fig. 5b. Initially, Fe undergoes oxidation to Fe_3O_4 in water in the presence of HCO_3^- to form a great amount of hydrogen which simultaneously *in situ* reduced Fe_3O_4, creating more active sites on the surface of Fe_3O_{4-x}. Subsequently, the generated hydrogen and HCO_3^- become activated upon adsorption on the Fe_3O_{4-x} surface. Following this, the activated H on the Fe_3O_{4-x} surface attacks C=O, resulting in the release of the hydroxyl group from HCO_3^-. Ultimately, this process leads to the formation of formate accompanied by H_2O. Furthermore, DFT calculations suggest that the $Fe–H^{\delta-}$ species is formed *via* the dissociation of water[73] (Fig. 5c and d). The Mulliken charge of H in the iron hydride was −0.135 in the HCO_3^- hydrogenation process, wherein a C–H bond forms in a transition state through the attack of $H^{\delta-}$ on $C^{\delta+}$. Ultimately, a $HCOO^-$ species was generated with an energy barrier of 16.43 kcal mol^{-1}.

In addition to formic acid production, C_2 and C_{2+} products were also synthesized from hydrothermal CO_2 reduction using Fe as the reductant., With RANEY®-Ni instead of Ni powder, the resulting *in situ* RANEY®-Ni/Fe_3O_4 acted as a bifunctional catalyst, facilitating the production of acetate.[34] A mechanistic study reveals that Fe_3O_4 is active for the formation of *in situ* hydrogen from water and in synthesizing formate, while the RANEY®-Ni site enhances the intermediate CO and its adsorption, leading to further hydrogenation to methylene. Subsequently, acetate was produced through the combination of formate and methylene on the RANEY®-Ni surface.

Moreover, long-chain hydrocarbons (up to C_{24}) were for the first time synthesized using Fe as the reductant and Co as the catalyst in a hydrothermal environment.[25] At 300 °C, the *in situ* formed Fe–OH, confirmed by *operando* infrared spectroscopy, enhanced CO adsorption on the Co site, thereby favoring further reduction to long-chain hydrocarbons (as shown in

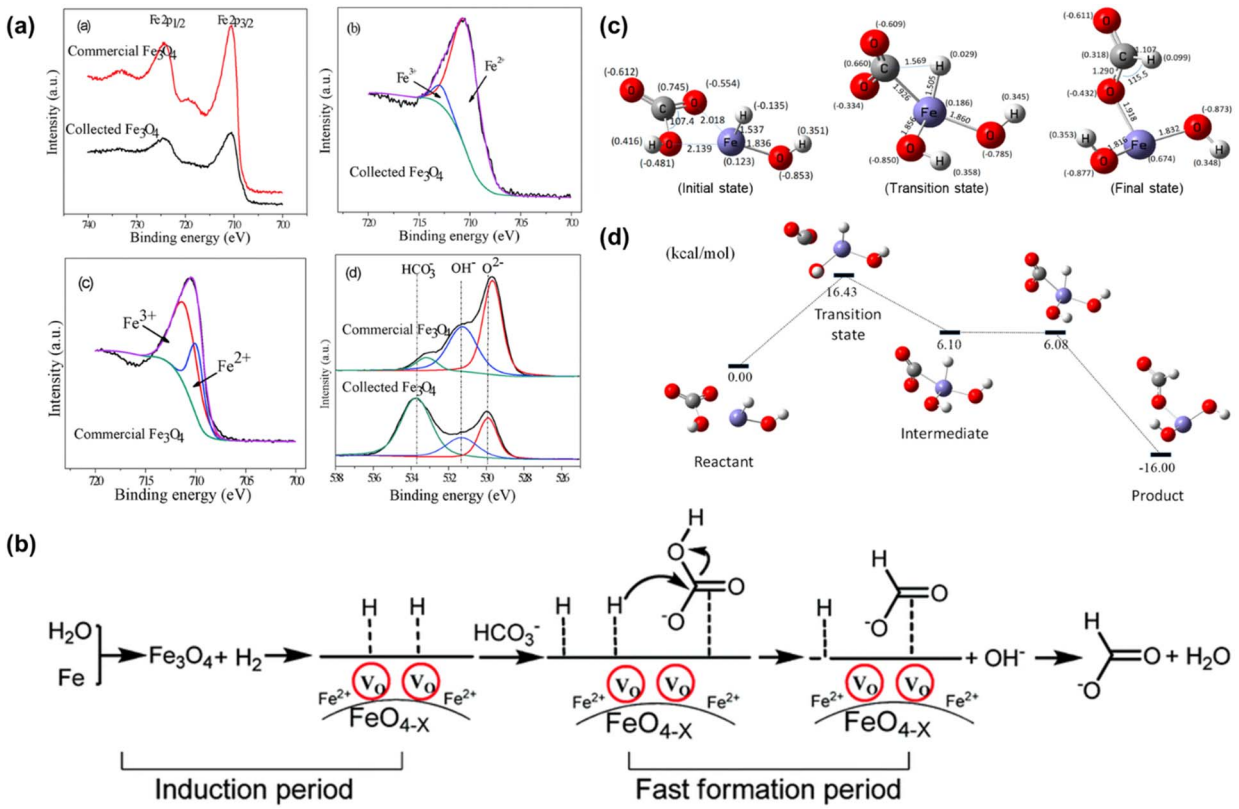

Fig. 5 (a) X-ray photoelectron spectra of collected and commercial Fe_3O_4; (b) proposed mechanism of $NaHCO_3$ reduction into formate with Fe.[52] This figure has been reproduced from ref. 52 with permission from The Royal Society of Chemistry, copyright 2016. (c) Optimized geometric parameters of the initial, transition and final states of HCO_3^- reduction with Fe. (d) Potential energy diagram for $HCOO^-$ production from HCO_3^- reduction with Fe.[73]

Fig. 6). It should be noted that under these hydrothermal conditions, the traditional issue of water-induced deactivation of Co can be inhibited by bicarbonate-assisted CoO_x reduction, leading to the formation of honeycomb-native Co nanosheets as a new motif. Accordingly, the Co^0 promoter responsible for synthesizing long-chain hydrocarbons is extraordinarily stable when coupled with Fe–OH formation.

3.2 Hydrothermal CO_2 reduction with Zn

When the reductant switched from Fe to Zn, methanol can be directly generated from the hydrothermal conversion of CO_2, with HCl playing a crucial role. Huo *et al.*[28] found an increase in methanol yield from 0.6% to 4.2% as the HCl concentration increased from 0.5 M to 2 M, and a maximum methanol yield of 11.4% was achieved at 350 °C for 3 h using 70 mmol Cu, 60 mmol Zn, and 2.0 M HCl. XRD analysis confirmed that Zn was oxidized to ZnO, while Cu maintained its valence. The proposed mechanism suggests that CO_2 is adsorbed on ZnO and subsequently undergoes a stepwise hydrogenation process to form methoxide species. Simultaneously, atomic hydrogen generated from water decomposition is supplied by spillover from Cu. Ultimately, methanol is formed through the hydrolysis of methoxide groups on ZnO, accompanied by the formation of H_2O as a by-product.

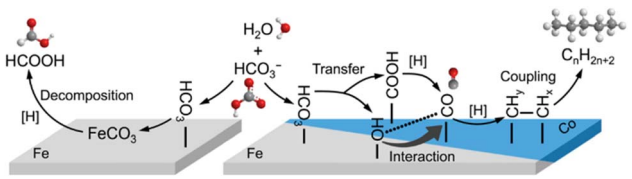

Fig. 6 Proposed hydrothermal reduction mechanism of $NaHCO_3$ into long-chain hydrocarbons.[25]

It is noteworthy that with the exclusive use of Zn for hydrothermal $NaHCO_3$ reduction, over 80% of formate was generated.[76] XRD results (Fig. 7a) revealed that almost all Zn underwent rapid oxidation to ZnO within 10 minutes. Additionally, the particle size of the resultant ZnO was found to be smaller than that of the original Zn powder. Thus, HCO_3^- can be effectively and selectively reduced to formate using solely Zn, without requiring a catalyst. Furthermore, the infrared spectrum indicated that Zn–$H^{\delta-}$ is an active intermediate resulting from the interaction between Zn and H_2O, as indicated in Fig. 7b. DFT calculations further confirmed that the Zn–$H^{\delta-}$ species is produced *via* the reaction of Zn with H_2O.[44] Specifically, it is in the form of H–Zn···O–H, attributable to the chemisorption of H_2, which drives the production of formic acid. Subsequently, $H^{\delta-}$ attacks the carbon center $C^{\delta+}$ of HCO_3^-, resulting in a bond formation with carbon in a transition state.

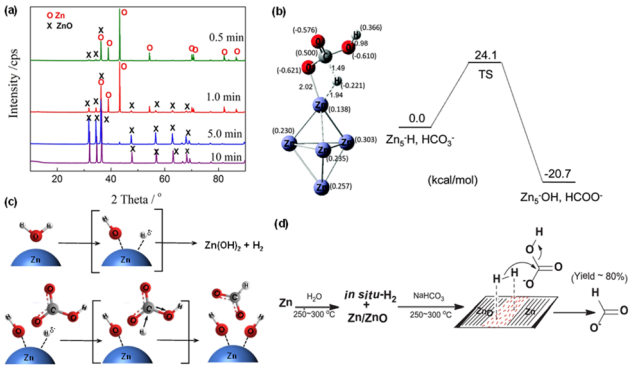

Fig. 7 (a) XRD patterns of Zn after $NaHCO_3$ hydrothermal reduction for different reaction times,[76] (b) the geometries of the transition state in reaction of Zn–H + HCO_3^- → Zn–OH + $HCOO^-$, (c) proposed SN_2-like mechanism for the formation of $HCOO^-$.[44] This figure has been reproduced from ref. 44 with permission from The Royal Society of Chemistry, copyright 2016. (d) Proposed autocatalytic mechanism of Zn/ZnO formed in water splitting for the conversion of CO_2 to formic acid with Zn.[77] This figure has been reproduced from ref. 77 with permission from Elsevier, copyright 2017.

Finally, the OH^- species dissociates, leading to the formation of $HCOO^-$ through an SN_2-like mechanism (Fig. 7c). Owing to the reversible nature of ZnO reduction and Zn oxidation, Zn–$H^{\delta-}$ formation occurs *via* the oxidation of Zn in water followed by hydrogen adsorption on ZnO. During the initial stages of the reaction, this *in situ* generated hydrogen adsorbs on ZnO surfaces and at the Zn/ZnO interface, where oxygen vacancies play a key role in hydrogen activation. The activated hydrogen subsequently nucleophilically attacks bicarbonate ions, with $H^{\delta-}$ added to the carbon of C=O, resulting in the formation of formate. This process, in which the autocatalytic mechanism at the Zn/ZnO interface is critical, is pivotal for the effective conversion of HCO_3^- into formate (as shown in Fig. 7d).[77]

Wang *et al.*[78] investigated the catalytic activity of various metals (Cu, Fe, Sn) in the hydrothermal reduction of CO_2 using Zn powder. Copper demonstrated the highest catalytic activity for formic acid production, achieving a yield of up to 61%. Zhong *et al.*[79] explored a method for converting bicarbonate into formate using nickel (Ni) and zinc/zinc oxide (Zn/ZnO). The process involves Ni playing a key role in enhancing the formation of oxygen vacancies at the Zn/ZnO interface. The study showed an impressive 81% yield of formate from bicarbonate at 225 °C, representing a significant improvement over the previous research without catalysts, which required 300 °C as the reaction temperature.

Liu *et al.*[80] found that formic acid could also be converted to methanol with Zn as the reductant and Cu as the catalyst. The highest methanol yield was 32% at 300 °C for 5 h utilizing 6.5 mmol Cu and 12 mmol Zn. In this reaction, H_2 was derived from both formic acid decomposition ($HCOOH = CO_2 + H_2$) and water splitting, coupled with Zn oxidation to ZnO. Subsequently, the newly generated H_2 dissociated into H(*a*) on the surface of Cu/ZnO and H(*a*) interacted with oxygen atoms in ZnO to produce H_2O, resulting in the formation of an oxygen vacancy in ZnO_{1-x}. Following this, CO_2 adsorbed on the oxygen vacancies of ZnO_{1-x}, and residual H(*a*) attacked the C–O bond near Zn to form ZnO–C–O. Therefore, the catalytic cycle concluded with the regeneration of Cu/ZnO and the formation of CH_3OH.

4 Hydrothermal CO_2 reduction with biomass or polymer wastes

Biomass is defined as all organic substances originating from plants, encompassing algae, trees, and crops. The composition of biomass differs based on its source but typically includes a wide range of organic compounds like lignin, proteins, carbohydrates (such as cellulose, starch, hemicellulose), and lipids. These compounds are characterized by functional groups such as hydroxyl (–OH), aldehyde (–CHO), or amino (–NH_2) groups. This section commences with a comprehensive discussion of the hydrothermal reduction of CO_2 by carbohydrates and their derivatives, and then transitions to examining protein-containing biomass such as microalgae and finally lignin. Ultimately, the scope of reductants expands from biomass to polymer wastes, which share similar functional groups like hydroxyl (–OH), with the aim of broadening the range of reducing agents to more economically viable sources.

4.1 Hydrothermal reduction of CO_2 by hydroxyl containing alcohols

Studies of CO_2 reduction with carbohydrates as reductants began with the examination of hydroxyl containing chemicals, given that carbohydrates are characterized by their polyhydroxy structure, and methanol as the simplest alcohol was selected as a representative. Wang *et al.*[35] found that formate can be successfully produced through $NaHCO_3$ reduction with methanol. Thermodynamic analysis showed that this process is favorable even at 453 K (eqn (1)).

$$CH_3OH + 2HCO_3^- \rightarrow HCOOH + 2HCOO^- + H_2O \quad (1)$$

$$\Delta_r H^\theta\ (298\ K) = -74.7\ kJ\ mol^{-1};\ \Delta_r G^\theta\ (298\ K) = -32.1\ kJ\ mol^{-1}$$

$$\Delta_r H^\theta\ (453\ K) = -49.7\ kJ\ mol^{-1};\ \Delta_r G^\theta\ (453\ K) = -15.8\ kJ\ mol^{-1}$$

A formate yield of 68% was achieved in hydrothermal $NaHCO_3$ reduction with methanol at 180 °C using a $Pd_{0.5}Cu_{0.5}$/C catalyst. ^{13}C-qNMR analysis was conducted to distinguish and quantify formate production from $NaHCO_3$ and CH_3OH. Approximately 55% of the formate originated from HCO_3^- reduction, while the remaining 45% resulted from CH_3OH oxidation. The superiority of $Pd_{0.5}Cu_{0.5}$/C catalyst was concluded not only due to its cost-effective characteristic of combining Pd and Cu but also to its role in enhancing hydrogen production and subsequent formate generation by altering the electronic structure of Pd by Cu. XPS analysis confirmed synergistic interactions between Pd and Cu. Specifically, the Pd 3d peaks in the alloy exhibited a lower binding energy compared

to those in Pd/C, indicating electron transfer from Cu to Pd. This electron shift modifies the electronic structure of Pd, reducing the hydrogen binding energy on its surface, thereby enhancing catalytic hydrogen generation, as shown in Fig. 8a. Furthermore, the altered Pd d-band center, distanced from the Fermi level due to Cu integration, lowers the formate adsorption energy, thus facilitating its production and selectivity in HCO_3^- reduction.

Operando hydrothermal ATR-FTIR studies, as detailed in Fig. 8b, revealed the transformation of reactants during the $Pd_{0.5}Cu_{0.5}$/C-catalyzed reaction. An increase in temperature and reaction time was found to enhance formate production. A blue shift observed in the peaks of the methanol C–O bond at 1110 and 1082 cm^{-1} suggested its oxidation to formaldehyde. This implies a mechanism in which CH_3OH oxidizes to HCHO, generating H_2, and then HCHO reacts with H_2O to produce H_2 and HCOOH. The adsorption of H_2 and HCO_3^- on $Pd_{0.5}Cu_{0.5}$/C results in formate formation through a nucleophilic attack on the C=O bond and C–OH bond cleavage. The potential reaction mechanism proposed for methanol and bicarbonate reaction under hydrothermal conditions *via* $Pd_{0.5}Cu_{0.5}$/C catalyst is illustrated in Fig. 8c. Furthermore, the study explored the reactivity of ethanol, 1-propanol, and 1-butanol in reducing $NaHCO_3$ to formate, testing the general feasibility of alcohols. These alcohols demonstrated activity comparable to methanol while being converted into their respective acids. Interestingly, the reactivity of these alcohols was found to increase marginally with the elongation of their carbon chain.

In addition to examining hydroxyl groups on terminal carbon atoms, isopropanol, the simplest secondary alcohol, was also chosen as a reductant for hydrothermal CO_2 reduction, with its operational parameters and reaction mechanism systematically investigated.[81] The formate yield was observed to gradually increase with the increase in CO_2 quantity, temperature, and reaction time. Conditions of 300 °C and 240 minutes were determined to be optimal. However, a moderate NaOH concentration was necessary to produce formate, as the base aids in improving the enthalpy of CO_2 reduction, while excess base can result in CO_2 conversion to Na_2CO_3. Generally, a formate yield of approximately 70% was achieved under conditions of 300 °C, 0.25 mol per L isopropanol, 1.0 MPa CO_2, and 0.75 mol per L NaOH. Drawing on the traditional Meerwein–Ponndorf–Verley (MPV) hydrogen-transfer reduction mechanism, which involves a cyclic transition state and the catalytic role of water molecules, a potential mechanism is proposed, as shown in Fig. 8d. Initially, two hydrogen bonds form between three molecules (isopropanol, H_2O, and HCO_3^- or CO_2 resulting from the decomposition of $NaHCO_3$), rendering the carbonyl-carbon of HCO_3^- or CO_2 and the hydride of isopropanol more electropositive. Subsequently, the hydride from isopropanol attacks the carbonyl-carbon of HCO_3^- or CO_2, leading to the formation of a cyclic transition state. Ultimately, following the intramolecular hydride shift, formate and acetone are produced, with the recovery of water molecules.

Beyond methanol and isopropanol, hexanol and glycerin, which possess multiple hydroxyl groups, were also utilized for hydrothermal CO_2 reduction. Yang *et al.*[40] found that operating parameters significantly impacted CO_2 conversion. Specifically, the formic acid yield linearly increased with the initial CO_2 loading, and a similar trend was observed for water filling, reaction time, and temperature. However, an optimal pH value was necessary to produce formic acid. The yield of formic acid dramatically increased from a pH of 6.5 and peaked at a pH of 7.5, but excessive alkalinity could result in the conversion of CO_2 to Na_2CO_3.[81] During this process, a maximum yield of 76% for formic acid was obtained.

Under alkaline hydrothermal conditions, the reaction of glycerol with $NaHCO_3$ primarily yields pyruvate, glycolate, lactate, formate, and acetate. It is noteworthy that glycolate was initially identified in reactions involving other polyols with $NaHCO_3$. In these reactions, formate tends to yield CO_2 through decarboxylation in the liquid phase. Wang[82] combined the results of previous research[32,83–85] and outlined three main competitive pathways for glycerol transformation: reduction of HCO_3^- and simultaneous conversion of glycerol (the lower pathway in Fig. 9), self-degradation of glycerol in alkaline media to lactate (the middle pathway in Fig. 9), and reverse aldol condensation yielding glycolate, formate, and lactate (the upper pathway in Fig. 9). For the simultaneous reduction of HCO_3^- and conversion of glycerol, Shen[32,86] further proposed a potential transfer hydrogenation mechanism where glycerol first undergoes dehydration to produce 2-hydroxypropanone, followed by keto–enol tautomerization to acetol. In the second step, potential hydrogen bonding between three molecules (acetol, water, and CO_2) enhances the electropositivity of the carbonyl carbon on CO_2 and the hydride ion on acetol. The hydride ion then attacks the carbonyl carbon, forming a cyclic

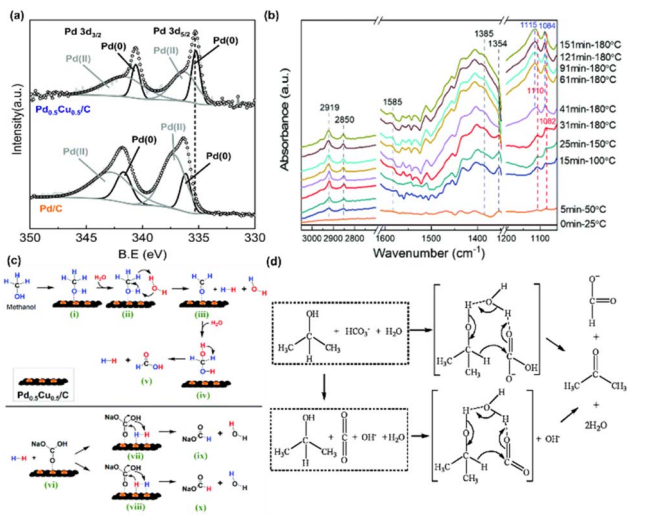

Fig. 8 (a) XPS spectra of Pd 3d in $Pd_{0.5}Cu_{0.5}$/C and Pd/C, (b) *operando* ATR-FTIR subtraction spectra recorded during $NaHCO_3$ reduction with methanol, (c) reaction mechanism of HCO_3^- reduction into formate with methanol in water on the $Pd_{0.5}Cu_{0.5}$/C catalyst.[35] This figure has been reproduced from ref. 35 with permission from The Royal Society of Chemistry, copyright 2021. (d) Possible mechanism for hydrogen-transfer reduction of $NaHCO_3$ with isopropanol.[81] This figure has been reproduced from ref. 81 with permission from The Royal Society of Chemistry, copyright 2011.

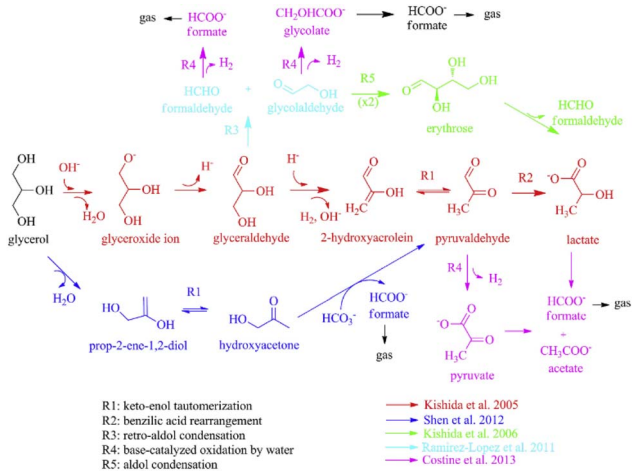

Fig. 9 Possible reaction mechanisms of hydrothermal reduction of HCO_3^- by glycerol.[82] This figure has been reproduced from ref. 82 with permission from Elsevier, copyright 2016.

transition state and ultimately yielding pyruvaldehyde and formate with the generation of a water molecule.

Catalysts are crucial in the glycerol-driven reduction of bicarbonate. In the reduction of bicarbonate using Ru/ZrO_2 catalysts and employing biodiesel waste glycerol as a reductant, a maximum formate yield of 25.1% was achieved, which is a significant increase compared to the mere 4.2% yield observed in the absence of catalysts.[87] The ruthenium component in the catalyst not only facilitates glycerol dehydrogenation but also enhances the hydrogenation of HCO_3^-. When employing the Pd/AC catalyst in the bicarbonate reduction with glycerol, the conversion of glycerol to lactate at 240 °C results in yields up to 55%, while simultaneously producing approximately 30% formate.[88] The reaction encompasses two potential hydrogen transfer pathways: glycerol dehydrogenation forming H_2 gas, which then hydrogenates bicarbonate, or direct transfer of hydrogen from glycerol to bicarbonate. Both pathways are catalyzed on the active sites of the Pd catalysts. For direct hydrogen transfer, firstly, the hydrogen donor dehydrogenates to form a palladium hydride, which then transfers the hydride to the hydrogen acceptor; secondly, the hydrogen donor and acceptor co-adsorb onto the Pd surface, enabling direct hydrogen transfer on the catalyst surface without forming hydrides.

Jaedeuk Park[89] devised and evaluated a two-pot/two-step transfer hydrogenation method (2P2S) for CO_2 reduction with glycerol. This method represents a comprehensive conversion process utilizing two reactors. The 2P2S method not only enhanced the yields of lactate and formate but also streamlined product purification and separation, ultimately producing lactate and formate or methyl formate (MF) while reducing the consumption of sulfuric acid (H_2SO_4) and potassium sulfate (K_2SO_4) waste, offering an environmentally friendly production route. Techno-economic and life cycle assessments reveal that the utilization of CO_2 is crucial for attaining significant economic benefits and minimizing climate change impact. Case studies demonstrate the lowest minimum product selling price (MPSP) of $1.25 per kg LA and the highest net present value (NPV) of $33.6 million, showing the economic competitiveness of the process. Moreover, the process significantly reduces material costs, as CO_2 utilization in the lactate and methyl formate production pathways reduces sulfuric acid usage and generates internal potassium bicarbonate ($KHCO_3$) through recycling.

4.2 Hydrothermal reduction of CO_2 by carbohydrates

As glucose is the primary product of lignocellulosic biomass hydrolysis, the reduction of CO_2 with glucose was systematically investigated. Yang *et al.*[90] achieved 54% formate yield under conditions of 0.125 mol per L glucose and 3 mol per L $NaHCO_3$ at 300 °C, employing a two-step reaction strategy. They proposed that the aldehyde group of glucose reduces HCO_3^- to $HCOO^-$ *via* a direct hydrogen transfer mechanism concurrently with the oxidation of glucose to gluconic acid. Subsequently, gluconic acid undergoes direct α-cleavage, resulting in the formation of formate and pentose (C_5 aldose). Further reactions lead to a gradual reduction in the carbon number of pentose, followed by a mechanism identical to the aforementioned process, culminating in the production of formate. As depicted in Fig. 10, this process results in a total of twelve formate and formic acid molecules originating from the reduction of $NaHCO_3$ by glucose (pathway I). Conversely, side reaction pathways (pathway II) also play a role in this reaction. Under hydrothermal conditions, the produced pentose (C_5 aldose) may undergo dehydration, keto–enol tautomerism, retro-aldol reactions, and benzilic acid rearrangement due to the long carbon chain, and eventually converts to products such as glyceraldehyde or acetaldehyde, which reduce $NaHCO_3$ to yield formate with themselves oxidized to lactic acid and acetic acid. Through this pathway, only two molecules of $NaHCO_3$ can be reduced. To optimally minimize the influence of side reactions, Yang *et al.*[90] developed a two-step reaction strategy focusing on cutting the carbon chain of glucose or cellulose, which could minimize the side reactions of multi-carbon aldoses. With this strategy, as high as 74% formate yield of $NaHCO_3$ reduction with direct use of cellulose was achieved.

Support for the direct hydrogen transfer mechanism was provided by *operando* hydrothermal diffuse reflectance infrared

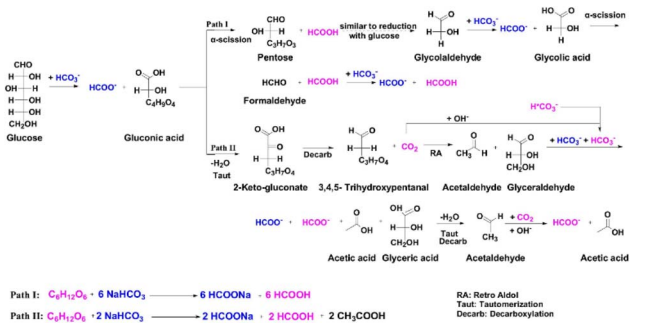

Fig. 10 Proposed reaction pathways of $NaHCO_3$ reduction with glucose.[90]

Fourier transform spectroscopy (OH-DRIFTS). Signals of formaldehyde and glycolic acid indicated glycolaldehyde (the intermediate of glucose) oxidation, which aids $NaHCO_3$ reduction, in assistance with the above proposed reaction pathway. The ν(C–H) signal of formate exhibited a blue shift, indicative of an elevated C–H bond energy. This enhanced C–H bond energy, likely caused by another functional group linked to the C atom, is attributed to the inductive effect dispersing the electron cloud of the central C atom, suggesting orthoformate formation, which forms formate through loss of H_2O. This shift, absent in $NaHCO_3$ reduction with gaseous H_2, directly proves $NaHCO_3$ reduction *via* hydrogen transfer between the aldehyde group of glucose and $NaHCO_3$.

Andérez-Fernández and colleagues[91] achieved formate yields of 65% for glucose and 35% for fructose at 300 °C, with 0.05 mol per L reactants and 0.5 mol per L $NaHCO_3$. They elucidated the reasons behind the yield disparity, attributing it to the decomposition of glucose into three C_2 molecules (such as glyoxal) and fructose into two C_3 molecules (like glyceraldehyde and pyruvic acid). It was discovered that under hydrothermal conditions, sugars initially undergo retro-aldol reactions or dehydration, forming smaller compounds like 5-hydroxymethylfurfural (5-HMF) and furfural. These intermediates can also reduce $NaHCO_3$, yielding a formate production rate of 15%, and through a series of reactions, including dehydration, keto–enol tautomerism, retro-aldol reactions, and benzilic acid rearrangement, they eventually convert to products such as lactic acid, acetic acid, and formaldehyde. In the early stages of the reaction, formic acid is directly produced from formaldehyde *via* dehydrogenation. As the reaction progresses, ^{13}C-NMR analysis detects formate from $NaHCO_3$ reduction gradually replacing the formic acid from organic matter. The proposed reaction mechanism includes hydrogen transfer and redox reactions between formaldehyde and $NaHCO_3$. Under hydrothermal conditions, formaldehyde may decompose through Cannizzaro reaction or dehydrogenation, generating formic acid and hydrogen, with the latter reacting with $NaHCO_3$ to form formate. This mechanism also involves a collection of reversible reactions during which formic acid and formaldehyde decompose into CO, CO_2, and H_2 at high temperatures, leading to a decrease in the total formate yield.[92]

Subsequently, a continuous flow reactor with the capacity to process 1.2 liters of bicarbonate solution per hour was developed. At shorter reaction times, the primary mechanism involves the decomposition of glucose into formic acid and other by-products, while at longer reaction times, a higher yield of formate was produced from bicarbonate reduction. These results suggest that the reduction pathway of bicarbonate occurs through the oxidation of by-products rather than the direct oxidation of glucose itself, requiring a longer reaction time to achieve a higher proportion of formate produced from bicarbonate reduction. It is hypothesized that glucose decomposes into glyceraldehyde and glycolaldehyde, which then further break down into formaldehyde, a crucial intermediate in the reaction with bicarbonate to produce formate. Other final products include acetic acid and lactic acid, alternative products of the decompositions of glyceraldehyde and glycolaldehyde.[93]

Using a Pd/AC and Pt/AC bimetallic catalyst in ethanol–water solvents at room temperature, Ding *et al.* obtained a 46% yield of formate and 21% yield of sorbitol by coupling glucose dehydrogenation with CO_2 hydrogenation. The key intermediate, ethyl carbonate, formed in basic aqueous ethanol, is crucial for the hydrogenation reaction. The reaction yields are significantly influenced by the initial pH and the amounts of glucose, ammonium carbonate, and KOH additives; the optimal pH for maximizing formate yield is around 11.73.[95] Oh *et al.* further found that the addition of alcohols significantly enhanced the catalytic activity.[94] A 50% 2-propanol solution exhibited the highest formic acid yield of 30.5%. Alkali metal carbonates showed superior catalytic activity compared to bicarbonates, with larger alkali metal cations effectively increasing the yield due to higher salt solubility. The presence of large alkali metal cations or alcohols enhanced reactivity by increasing the interaction between reactants and the metal surface, attributed to the water structure-breaking effect, as illustrated in Fig. 11. This was particularly crucial for glucose anions and bicarbonate, indicating a stronger hydration sphere for anions than neutral molecules. By exploiting the dual effect of large alkali metal cations and alcohols, the carbohydrate sources could be extended to galactose and lactose.

4.3 Hydrothermal reduction of CO_2 by microalgae or lignin

In addition to carbohydrate biomass, microalgae are regarded as a third generation of biomass energy due to advantages such as rapid growth rate, high photosynthetic efficiency, and no competition for food resources. In contrast to carbohydrate biomass, the chemical compositions of microalgae include abundant lipid and protein. The former is comprised of glycerol and carboxylic acid, for which the reduction of CO_2 is

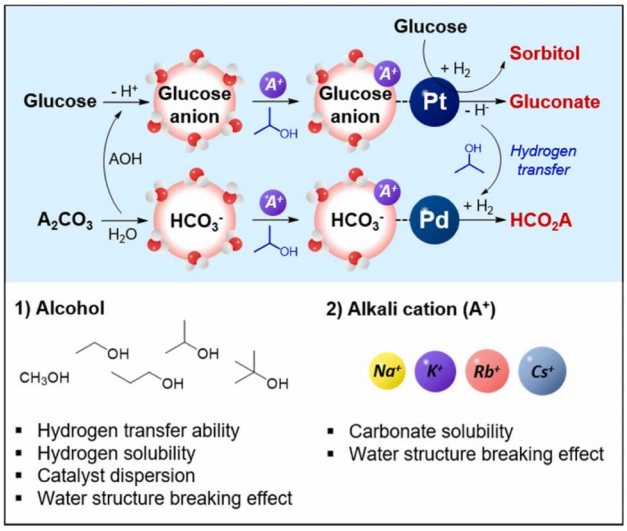

Fig. 11 The proposed reaction mechanism for simultaneous transformation of glucose and alkali carbonate.[94] This figure has been reproduced from ref. 94 with permission from Elsevier, copyright 2022.

summarized with emphasis on the reductive capacity of hydroxyl group, and the latter is characterized by the amino group, which is also a reductive functional group in addition to the hydroxyl and aldehyde groups. However, few studies have recognized and concentrated on the utilization of the amino group in biomass, particularly in driving CO_2 reduction. In this section, we summarize the hydrothermal reduction of CO_2 with amino-containing model compounds and actual microalgae biomass.

Yang *et al.*[39] conducted pioneering research on the feasibility of hydrothermal CO_2 reduction using *Spirulina*, a commonly known microalga. Comparative experiments demonstrated that the sole conversion of *Spirulina* yielded over 15 complex products, primarily including organic acids (acetic acid, formic acid, and propionic acid), chain amides (*N*-ethyl-acetamide, *N*-methyl-acetamide, and acetamide), *N*-substituted 2,5-diketopiperazines (*N*-ethyl-2,5-diketopiperazine and *N*-methyl-2,5-diketopiperazine), and lactams (*N*-ethyl-2-pyrrolidinone, *N*-methyl-2-pyrrolidinone, 2-pyrrolidinone, 2-piperidinone, and 2-oxoazepane). However, the distribution and selectivity of products altered when *Spirulina* reacted with $NaHCO_3$, and the yields of organic acids and lactams increased obviously, with a sharp decrease in the production of chain amides and diketopiperazines, and, combined with ^{13}C-NMR analysis, the production of formate from the reduction of $NaHCO_3$ was confirmed. Systematic research on the reaction parameters indicated that *Spirulina* conversion was enhanced by increasing $NaHCO_3$ concentration. Elevating the temperature and extending the reaction time can enhance the conversion of both *Spirulina* and $NaHCO_3$. In this instance, 325 °C and 2 h represented the optimal conditions for formate production. The addition of NaOH augmented formate production from $NaHCO_3$, while its effect on the conversion of *Spirulina* was limited. After acknowledging the possible reaction mechanism, the range of reductant substrates was expanded from *Spirulina* to *Chlorella* and microalgae residue, demonstrating the general applicability of the reaction protocol.

Amino acid is easily obtained from protein-rich microalgae biomass. Li *et al.*[96] chose L-alanine as the model chemical to verify the feasibility of hydrothermal CO_2 reduction by amino acid. In the presence of $NaHCO_3$, there was a significant increase in formate yield (9.3%), a finding also corroborated by ^{13}C-NMR analysis with $NaH^{13}CO_3$ as the reactant. A screening of active metal catalysts (Cu, Co, Ni, Ru, Pd, and Pt) and suitable supports (SiO_2, CeO_2, ZrO_2, ZnO, and gamma-Al_2O_3) for hydrothermal $NaHCO_3$ reduction with L-alanine was conducted, where Pd/γ-Al_2O_3 exhibited higher activity, achieving a formate yield of 49.0% under conditions of 0.8 mol per L L-alanine and 0.8 mol per L $NaHCO_3$ at 325 °C for 2 hours with 0.08 g of 5% Pd/γ-Al_2O_3.

As depicted in Fig. 12a and b, OH-DRIFTS was also utilized to ascertain the reaction mechanism of amino groups reducing $NaHCO_3$. The peaks at 3500–3300 cm^{-1}, exhibiting a growing negative variation pattern, were attributed to the $-NH_2$ group of L-alanine, indicating continuous consumption of $-NH_2$ in L-alanine during the reaction.[97] Conversely, the NH_4^+ signal in the range of 3000–2800 cm^{-1} exhibited a nearly unchanged state

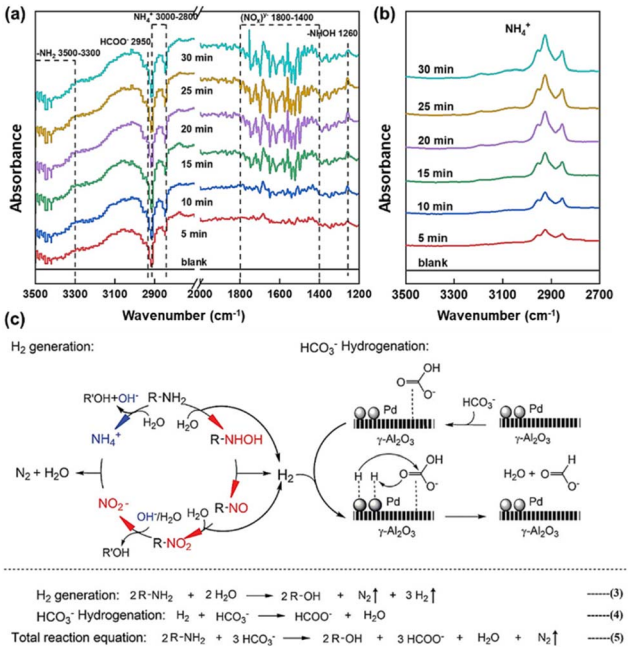

Fig. 12 OH-DRIFTS spectra of L-alanine reaction with $NaHCO_3$ (a) or without $NaHCO_3$ (b) (only the absorbance signal for NH_4^+ was displayed in spectra (b)), (c) proposed reaction mechanism of $NaHCO_3$ hydrothermal reduction with L-alanine.[96] This figure has been reproduced from ref. 96 with permission from American Chemical Society, copyright 2021.

after 5 minutes, while this peak tended to intensify due to the hydrolysis of amido at a rapid rate, implying the continuous consumption of NH_4^+ over time. The signal at 1260 cm^{-1} was assigned to hydroxylamine (R–NHOH). Given that hydroxylamine is the product of $-NH_2$ oxidation, this signal provided direct evidence of $NaHCO_3$ reduction *via* $-NH_2$ oxidation. It is noteworthy that the R–NHOH peaks displayed an increasing and then decreasing trend, suggesting that R–NHOH was an intermediate in the $-NH_2$ oxidation process. Additionally, absorbances of N–O and NO_2^- were observed at 1642 cm^{-1} and 1570 cm^{-1}, respectively. Based on these results, the proposed mechanism of amino acid reduction of $NaHCO_3$ to formate is as follows (Fig. 12c). $-NH_2$ is first oxidized into hydroxylamine by releasing one molecule of H_2, and then hydroxylamine forms two molecules of H_2 by oxidizing to R–NO and R–NO_2. Subsequently, NO_2^- interacts with NH_4^+ (hydrolyzed from the amino acid) to generate N_2 and H_2O, with the concurrent formation of alcohols from the amino acid. Meanwhile, $NaHCO_3$ hydrogenation occurs on the catalyst surface, where *H is adsorbed on the Pd site and HCO_3^- is adsorbed on the support γ-Al_2O_3, leading to the reduction of $NaHCO_3$ to formate.[51]

The reduction efficiency of aromatic ring-containing lignin has also garnered attention. Andérez-Fernández[91] investigated the efficacy of CO_2 reduction using various lignin model compounds. Under the conditions of 300 °C for 180 minutes, phenol yielded only 2% formic acid yield. In contrast, higher formic acid yields were observed with resorcinol and catechol solutions (19% and 9%, respectively). The highest yield of 51% was achieved with a vanillin solution, followed by a 24% yield

with guaiacol. These results suggest that aromatic compounds possessing *ortho* or *para* hydroxyl groups exhibit greater CO_2 reduction activity. Oxidation by-products from lignin derivatives suggest that the reaction may proceed *via* a ring-opening mechanism. Vanillin is hypothesized to undergo Cannizzaro disproportionation to vanillic acid and vanillic alcohol, with the latter being involved in CO_2 reduction. Aromatic compounds in high-temperature water may be oxidized to quinone groups, which are prone to ring opening. The proposed CO_2 reduction mechanism involves oxidation through a cyclic transition state, wherein the hydrogen atom to be transferred is located on the hydroxyl group.

Apart from biomass, recent advancements have highlighted the potential of biomass polymer waste for CO_2 reduction. Specifically, a study[98] demonstrated that when 5.0 g per L sugarcane bagasse solution reacted with 42.0 g per L $NaHCO_3$ at 250 °C for 3 h, a maximum formate yield of 10% was achieved. Experiments using various bases, including NaOH and phosphate buffer, indicated that alkaline conditions favor biomass waste oxidation to acids while impeding the conversion of CO_2, dissolved as bicarbonates/carbonates. The addition of $NaHCO_3$ serves not only as a secondary carbon source, converted to formate, but also as an oxidant, thereby enhancing the conversion of biomass wastes into organic acids.

4.4 Hydrothermal reduction of CO_2 by polymer wastes

Plastics have revolutionized modern life due to their low cost and utility in a wide range of applications. Regrettably, the accumulation of artificial polymers in landfills and environment has led to a global pollution crisis,[99] which in turn has accelerated research on the conversion of plastic waste into value-added chemical products.[100,101] Recently, Ma *et al.* developed a process for the co-utilization of waste plastics and CO_2. They designed a triple-reaction coupling involving CO_2 hydrogenation, methanolysis of polyethylene terephthalate (PET), and hydrogenation of dimethyl terephthalate (DMT), effectively degrading PET and utilizing CO_2. As shown in Fig. 13a, CO_2 as a solvent precursor overcomes the thermodynamic limits of the reactions. CO_2 is hydrogenated to methanol, which then decomposes PET into DMT and ethylene glycol (EG). Subsequently, DMT is hydrogenated into higher-value chemicals such as dimethyl 1,4-cyclohexanedicarboxylate (DMCD) and *para*-xylene (PX). This coupled reaction significantly improves the yield of CO_2 hydrogenation or PET methanolysis by 2 to 7 times compared to uncoupled reactions. In addition, with tandem catalysis, a promotion of the synergistic coupling of CO_2 hydrogenation and PET methanolysis was achieved to produce valuable chemicals like cyclohexanedicarboxylate over Cu_4Fe_1-Cr_1 catalyst.[102]

Under hydrothermal conditions, a one-pot, two-step catalytic method using commercial Pd/C catalysts enabled the conversion of polyesters like polyglycolic acid (PGA), polyethylene terephthalate (PET), and poly(butylene adipate-*co*-terephthalate) (PBAT) with sodium carbonate into sodium formate, without external hydrogen. As shown in Fig. 13b, at 250–270 °C, polyesters undergo aqueous modification with Pd/C catalysts,

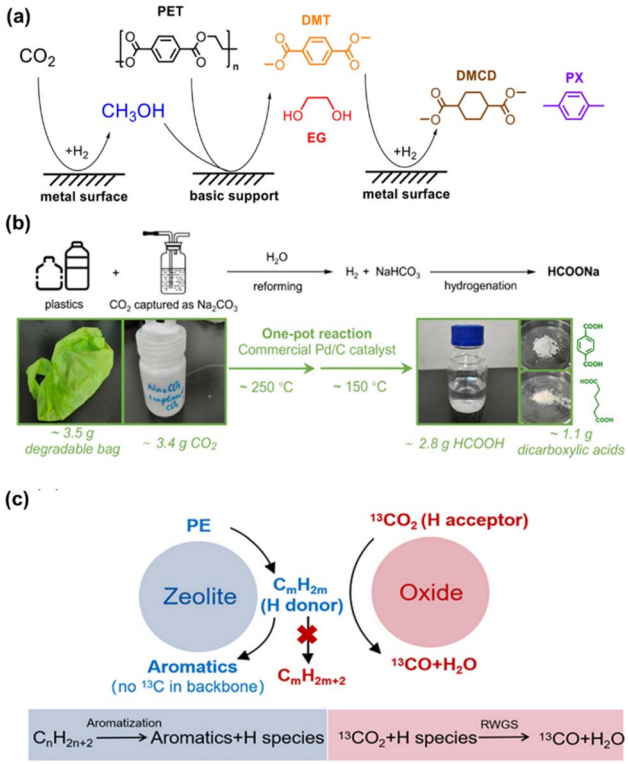

Fig. 13 (a) The scheme of CO_2 hydrogenation and PET degradation dual-promoted reaction system.[102] This figure has been reproduced from ref. 102 with permission from Wiley-VCH GmbH, copyright 2022. (b) Plastic and CO_2 in one pot, two-step catalytic conversion process.[103] This figure has been reproduced from ref. 103 with permission from American Chemical Society, copyright 2024. (c) Proposed mechanism for the coupling reaction of CO_2 with PE over composite catalyst.[104]

breaking down into smaller molecules. Subsequently, at 150 °C, the hydrogen generated in the first step is used for the hydrogenation of $NaHCO_3$. This technique effectively resolves the contradictions in reaction temperature and pressure between plastic reforming and $NaHCO_3$ hydrogenation, achieving a 79% yield of HCOONa.[103] Additionally, CO_2 facilitates the conversion of polyethylene (PE) into aromatics, achieving synergistic resource utilization, as shown in Fig. 13c. Utilizing Cu–Fe_3O_4 and Zn/ZSM-5 tandem catalysts at temperatures below 400 °C, an efficient conversion with 64.0% aromatic selectivity was achieved. This process not only exceeds the 50% theoretical limit of aromatic selectivity in PE aromatization but also, through ^{13}C isotope studies, confirms CO_2's role in the reverse water–gas shift (RWGS) process. CO_2, acting as a hydrogen scavenger and converting to CO, significantly reduces hydrogen transfer reactions in olefinic intermediates, decreasing the fraction of light alkanes and enhancing the formation of aromatic compounds. Notably, CO_2 does not participate in extending the carbon chain of aromatic compounds.[104]

Furthermore, the synergistic transformation of PVC plastics and CO_2 was achieved even without the use of any external metal-based catalysts. ^{13}C-NMR analysis was performed on the liquid sample derived from the reaction of $NaH^{13}CO_3$ and PVC.

As depicted in Fig. 14a, the labeling experiment using $NaH^{13}CO_3$ revealed a strong signal attributed to $H^{13}COO^-$ at a chemical shift of 171.1 ppm in the ^{13}C-NMR spectrum, confirming that formate originated from $NaHCO_3$.[105] Research on reaction characteristics indicated that higher temperatures (over 300 °C) and longer times (more than 8 hours) can lead to formate decomposition, and higher $NaHCO_3$ concentrations (more than 4 mmol) can cause an insufficient amount of PVC as the reductant. Under conditions of 125 mg PVC, 300 °C, 8 hours, 1 mmol $NaHCO_3$, and 2 mmol NaOH, approximately 16% formate yield was achieved.

FT-IR analysis was also utilized to investigate the reduction of bicarbonate to formate using PVC under various reaction conditions. In Fig. 14b, absorption signals of C=C and –OH stretching vibrations were observed at 1621 cm^{-1} and 3200–3700 cm^{-1}, respectively, while the absorption peak of the C–Cl stretching vibration disappeared following the reaction between PVC and NaOH. Collectively, these results indicate that the OH^- in water attacks the β-H and α-C of PVC, resulting in the formation of C=C, C=C–H, and CH–OH groups. Conversely, after the reaction of PVC with $NaHCO_3$ and NaOH, in contrast to the reaction of PVC with NaOH alone, the absorption peak of the C=O stretching vibration (1701 cm^{-1}) appeared, and the peak of the –OH stretching vibration decreased significantly with the addition of $NaHCO_3$, implying the formation of the CH–OH group through an SN_2 mechanism and its further conversion to C=O in the presence of $NaHCO_3$. Overall, the proposed reaction mechanism of $NaHCO_3$ for the hydrothermal reduction of $NaHCO_3$ to formate with PVC is depicted in Fig. 14c. Initially, dichlorination of PVC occurs under hydrothermal conditions, forming intermediate A by the elimination of OH^- attacking on the β-H and the substitution of OH^- attacking on the α-C; then, the *in situ* formed CH–OH is oxidized to C=O by HCO_3^-, while HCO_3^- is reduced to formate.

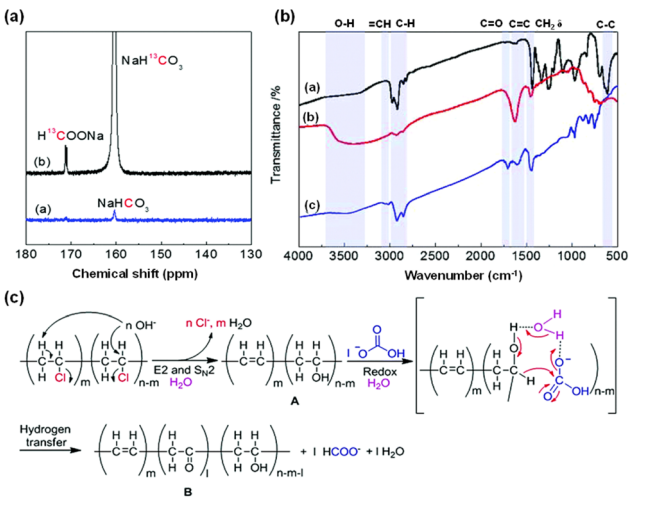

Fig. 14 (a) ^{13}C-NMR spectra of liquid samples for the reactions of PVC with $NaHCO_3$ or $NaH^{13}CO_3$, (b) FT-IR spectra of PVC before and after the reaction under different conditions ((b-a) pure PVC, (b-b) solid product for the reaction of PVC + NaOH, (b-c) solid product for the reaction of PVC + NaOH + $NaHCO_3$), (c) proposed mechanism of HCO_3^- reduction to formate using PVC under hydrothermal conditions.[105] This figure has been reproduced from ref. 105 with permission from The Royal Society of Chemistry, copyright 2020.

Additionally, hydrothermal CO_2 reduction using ethylene propylene diene monomer (EPDM) as a model compound for sulfur-containing rubber was conducted. The results showed that formic acid was the main product, and carboxylic acids with 2–4 carbon atoms were also formed.[45] It should be noted that a higher temperature of 400 °C was required, and, upon increasing the temperature to 450 °C, C_5–C_6 products were detected, during which a 20% CO_2 reduction efficiency was achieved. From the cracking of EPDM, straight-chain *n*-alkanes with more than nine carbon atoms were formed.

5 Roles of water in hydrothermal CO_2 reduction

The general feasibility of reductants for CO_2 reduction under hydrothermal conditions, ranging from metals to biomass and even plastics, indicates the unique property of HTHP water in invoking the reductive power. The commonly recognized advantages of HTHP water include: (1) the excellent solubility of organics and gases; (2) the increase in the concentration of H^+/OH^- ions which facilitates acid/base-catalyzed reactions; (3) the significantly reduced diffusion rate of supercritical water to nearly 1/100 that of liquid water; and (4) the weak interaction of hydrogen bonds among water molecules, which reduces mass transfer resistance at the interface, leading to efficient heat transfer, rapid mass diffusion, and an enhanced reaction rate. However, the mechanistic study of CO_2 hydrothermal reduction, particularly through *in situ* observations with FTIR, suggests that, in addition to these advantages, a potentially significant yet often overlooked homogeneous catalytic function of HTHP water might exist.

In hydrothermal CO_2 reduction with methanol, the role of water was investigated carefully.[35] Wang *et al.* discovered that water is crucial for the initial step of methanol activation, as no H_2 and HCHO were detected in the reaction with only methanol in the absence of water. Furthermore, the generation of H_2 from methanol, both with and without H_2O, was analyzed through DFT calculations. As depicted in Fig. 15a–c, the added H_2O molecule functioned as a proton acceptor, forming a deformed H_3O-cation-like conformation with the transition state hydrogen atom from the methanol molecule. This significantly reduced the activation energy required for ionic water dissociation. Consequently, the energy barrier for H_2 formation from methanol was lowered from 378 kJ mol^{-1} without H_2O to 220 kJ mol^{-1} with H_2O present (Fig. 15d). Additionally, an isotopic tracing reaction with D_2O substituting H_2O was conducted, with $NaH^{13}CO_3$ as the carbon source to differentiate formate from $NaHCO_3$ reduction. As illustrated in Fig. 15e and f, a peak corresponding to $D^{13}COO^-$ was distinctly observed in the D-NMR spectrum, consisting of two parallel peaks. The ^{13}C-NMR image revealed that the $NaH^{13}CO_3^-$ derived formate contained three parallel peaks attributed to the resonance effect between ^{13}C and D. The COSY spectrum of the liquid sample post-reaction between $NaH^{13}CO_3$ and methanol in D_2O is also

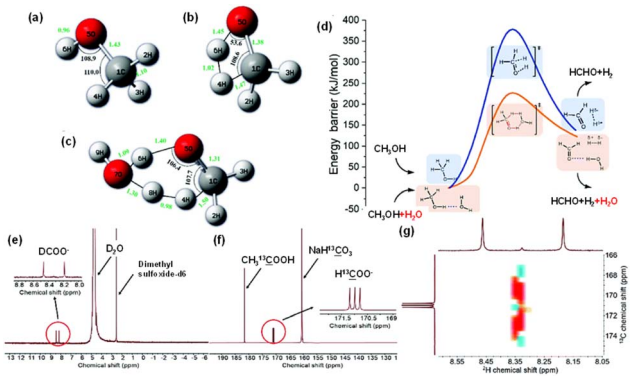

Fig. 15 Transition states (a–c) and energy profiles (d) for methanol dissociation into H_2 with or without H_2O ((a) methanol molecule, (b) the transition state without H_2O, (c) the transition state with H_2O, (d) the profile with H_2O as the promoter is depicted in orange, and the profile without H_2O is depicted in blue); (e) D-NMR, (f) ^{13}C-NMR and (g) COSY spectrum of the liquid sample after $NaH^{13}CO_3$ reaction with methanol in D_2O.[35] This figure has been reproduced from ref. 35 with permission from The Royal Society of Chemistry, copyright 2021.

depicted in Fig. 15g. These findings confirmed that the formate derived from $NaHCO_3$ reduction incorporated D from D_2O, and further analysis demonstrated that the final formate product consisted of nearly equal amounts of $H^{13}COO^-$ and $D^{13}COO^-$. Thus, the catalytic role of H_2O in methanol activation is substantiated and is in perfect alignment with the DFT calculations.

When PVC was used as a reductant, the reduction of $NaHCO_3$ to formate did not occur in the absence of water,[105] and high-temperature water is hypothesized to play a critical role in this process. Initially, hydrogen bonds are presumed to form among three molecules: dechlorinated PVC, H_2O, and HCO_3^-. This interaction is believed to increase the reactivity of the O–H bond in dechlorinated PVC and the C–O bond in HCO_3^-. Subsequently, the hydride ion from dechlorinated PVC is postulated to attack the carbonyl carbon of HCO_3^-, leading to a cyclic transition state. Finally, upon hydrogen transfer, formate and the C=O group are generated, and water molecules are recovered.

Furthermore, in Yang *et al.*'s study on CO_2 reduction with glucose, the OH-DRIFTS spectra of $NaHCO_3$ reduction with glycolaldehyde, a model compound of carbohydrates, revealed the presence of hydrated aldehyde groups in formaldehyde and glycolaldehyde which helped $NaHCO_3$ reduction through a hydrogen transfer mechanism, and a water molecule was recovered after formate generation. This result directly proved that water assists the hydrothermal reaction as a homogeneous catalyst. Specifically, when a –CHO group becomes hydrated, the reductive hydrogen attached to the central carbon becomes more nucleophilic, enabling it to reduce electron-deficient substances more easily.[106]

Consequently, when molecular water hydrates the –CHO group to form $-CH(OH)_2$, the reductive hydrogen of the aldehyde group becomes sufficiently active to directly attack $NaHCO_3$ molecules through hydrogen transfer. As shown in Fig. 16, a six-member ring transition state is formed with

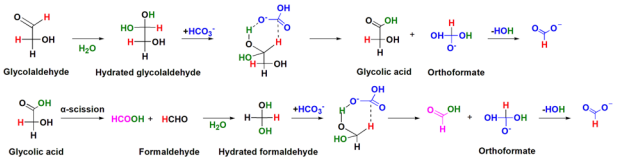

Fig. 16 Catalytic role of water in hydrogen transfer for $NaHCO_3$ reduction with glycolaldehyde. (Reactant $NaHCO_3$/its reduced $HCOO^-$ and glycolaldehyde formed HCOOH are depicted in blue and violet, respectively. Reductive hydrogen in glycolaldehyde is exhibited in red, and H_2O catalyzing the reaction is shown in green.)[107]

HCO_3^-, leading to the formation of a C–H bond between the highly activated hydrogen and HCO_3^- through nucleophilic addition to a C=O bond. Thereafter, HCO_3^- is reduced to orthoformate, which then releases H_2O to form formate to complete the catalytic cycle.

These results suggest that hydrothermal water can accelerate the reaction either by forming a bridge inside a molecule or between molecules or by hydrating reactants for higher activity. Indeed, the promoting role of water in reactions has been documented in several cases, such as by altering reaction pathways through the blocking of active sites or by forming intermediates or products with substrates *via* hydroxyl groups from water, thus creating alternative reaction paths.[108] The summarized catalytic function of HTHP water here may further expand the understanding of water's role in enhancing reactions and extend the scope of hydrothermal chemistry.

6 The assessment of carbon emission budget and efficiency of CO_2 reduction with renewable reductants under hydrothermal conditions

The summarized research demonstrated that multiple value-added chemicals or fuels can be produced from CO_2 hydrothermal conversion, as depicted in Fig. 17a, indicating the potential of applying the technology for large scale CO_2 conversion. To advance CO_2 reduction in meeting the requirements of net carbon benefit and high efficiency, a comparison of the summarized approaches from the reported methods of catalytic hydrogenation and photo/electro-catalyzed CO_2 reduction was performed. Fig. 17b demonstrates the efficiencies of various CO_2 catalytic methods for formic acid production. Iron powder, used for the hydrothermal reduction of CO_2 to formic acid, exhibits the highest efficiency. Additionally, compared to photo/electro-catalysis and hydrogenation catalysis, biomass and metal induced reduction of CO_2 not only offer the advantage of high efficiency but also simplicity and cost-effectiveness due to the absence of complex catalyst preparation. Fig. 17c displays the potential greenhouse gas (GHG) emissions throughout the lifecycle of different CO_2 catalytic methods. While photo/electro-catalysis aims for green and sustainable development, its low efficiency, the need for catalyst preparation, and the high energy demand of the entire system do not confer an advantage in CO_2 emission reduction. In the

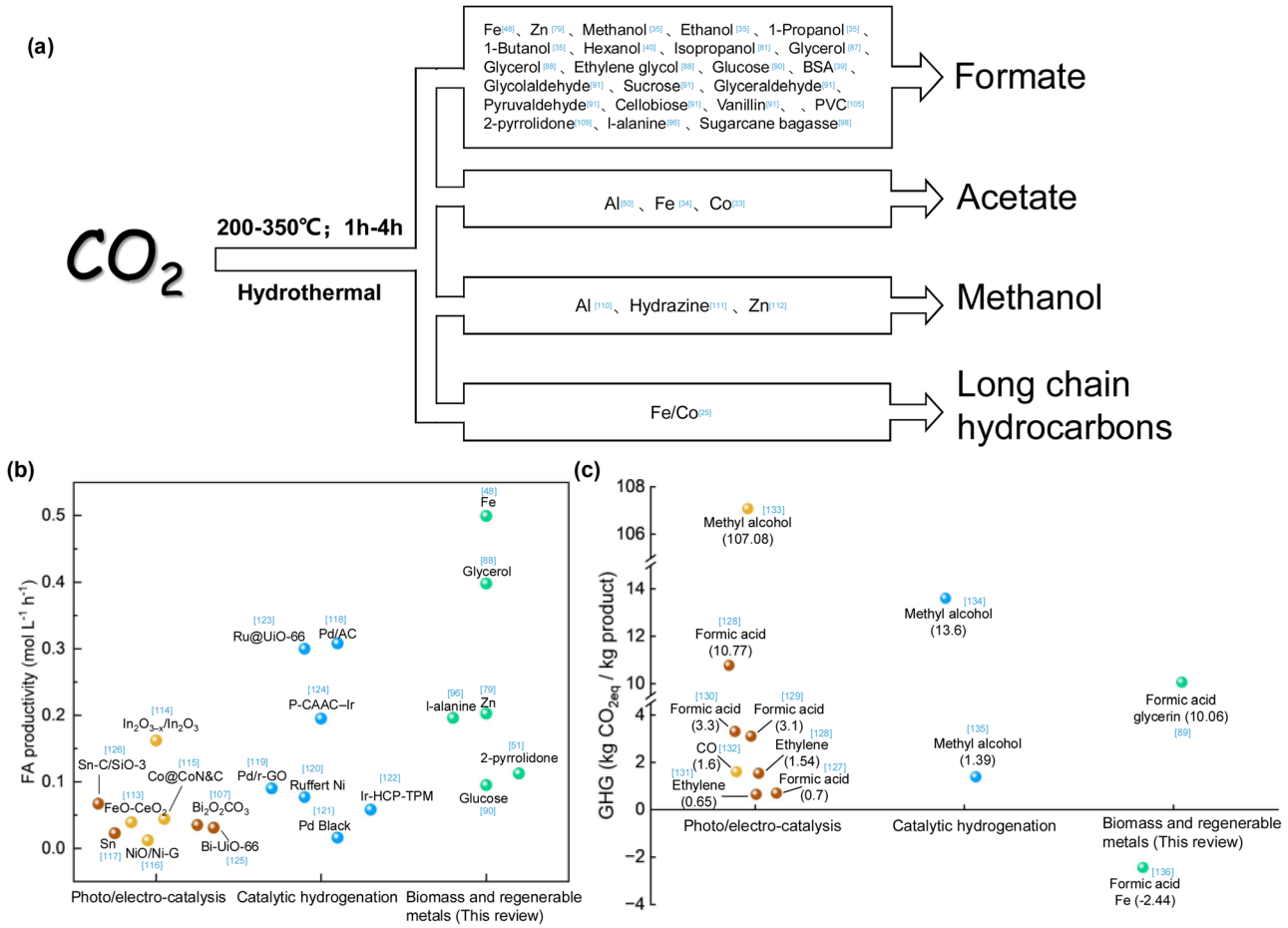

Fig. 17 (a) Main products that can be obtained by hydrothermal CO_2 conversion,[33–35,39,40,48,50,79,81,87,88,90,91,96,98,105,109–112] (b) comparison of formic acid production efficiency by different CO_2 catalytic methods,[48,51,79,88,90,96,107,113–126] (c) comparison of greenhouse gas emissions by different CO_2 catalytic methods[89,127–136] (yellow balls represent photocatalysis, brown balls represent electrocatalysis, blue balls represent catalytic hydrogenation, green balls represent biomass and regenerable metals).

hydrogenation catalysis process, the sources of CO_2 and H_2 and the boundaries considered in the life cycle assessment (LCA) significantly impact GHG emissions. For CO_2 reduction *via* biomass and regenerable metals, the system's lower dependency on electricity, the use of sodium hydroxide for effective CO_2 absorption, and the use of biomass or solar energy as the energy input contribute to its potential as a carbon-neutral technology. Moreover, implementing low-carbon energy sources and waste heat recovery methods can significantly reduce greenhouse gas emissions.

7 Challenges, prospects and conclusions

As an indispensable part in dealing with the threat of GHG emissions, CO_2 conversion into fuels or chemicals is considered a revolutionary technology for thoroughly coping with the issue and generating sustainable carbon sources without using the conserved fossil sources on Earth. Still far from practical implementation, CO_2 conversion approaches face formidable challenges in terms of renewable reductive sources, easy handling reaction systems, and readily accessible high efficiency. Specifically, (1) catalytic CO_2 hydrogenation exhibits the highest reaction efficiency, while the need for gaseous hydrogen compromises the net carbon benefit since industrial hydrogen production relies heavily on fossil fuels as the feedstock; moreover, the storage and transportation of high pressure gas also require large amounts of energy input;[137] (2) solar or electro induced CO_2 reduction could entirely or partly use solar energy as the energy input which promises the high prospect of achieving net carbon benefit; however, the efficiency of solar reactions is relatively poor now, and the competitive reaction of hydrogen evolution in electrochemical CO_2 reduction interferes with reaction selectivity; and (3) for solar-/electro-CO_2 reduction, delicate prepared catalysts or electrodes are inevitable, leading to difficulties in implementing the technology practically. Therefore, from the perspective of practical applications, it is urgent to develop efficient strategies to use renewable reductants and operable and scalable methods in CO_2 conversion to achieve the dual goals of efficient and net carbon benefit CO_2 reduction.

In this review, we comprehensively summarize the recent achievements of hydrothermal CO_2 reduction with renewable reductants, starting with the origin and advantages of

hydrothermal technology and the feasibility of certain metals, biomass, and organic waste as renewable reductants for CO_2 conversion. Moreover, we focus on the reaction characteristics and mechanisms to discuss whether the summarized technologies can overcome the existing challenges of CO_2 conversion. Specifically, we first classify the renewable reductants for efficient CO_2 reduction, including the metals Zn[9,41,51,56,77,80] and Fe,[29,32,34] biomasses as carbohydrates, microalgae and lignin, and organic solid waste as plastics. More importantly, the intrinsic advantages of hydrothermal CO_2 reduction are represented, for example, the self-catalytic process of metal induced CO_2 reduction, the high reducing capacity of an organic hydrogen source catalyzed by the hydrothermal environment, and the easily controlled reaction process by regulating the hydrothermal reaction settings. Although significant progress has been made in hydrothermal CO_2 reduction with renewable reductants, particularly by comparing the hydrothermal technology with existing approaches, and the advantages of hydrothermal conversion are demonstrated to satisfy the dual goals of high efficiency and net carbon benefit, the implementation of this method is still in the early stages and full of challenges. Thus, the following perspectives should be taken into consideration in future research.

First, for metal-initiated CO_2 reduction, although high efficiency can be achieved readily even without catalysts, the limited products species should be noted. Currently, the manufacture of C_1 products such as formic acid, methanol, and methane is sufficiently ready, while for multi-carbon products, such as hydrocarbons and multi-carbon acids, only certain reaction settings can achieve the target. Thus, it is urgent to screen and synthesize proper catalysts to break the bottleneck. Indeed, primary studies have shown that Co[25] and Ni are two feasible core metals for catalyzing carbon–carbon coupling in CO_2 hydrothermal reduction, and they have been demonstrated for hydrocarbon and acetic acid production. Moreover, due to the rigid reductive environment of hydrothermal reduction, the oxidation and consequent deactivation of Co or Ni based catalysts are avoided, which are the primary problems affecting the use of these two catalysts in other catalytic processes. However, other products have been scarcely observed, calling for further effort in exploiting more proper catalysts. Moreover, the abovementioned catalysts functioned with the assistance of *in situ* generated reductant oxides such as Fe_3O_4, while ZnO could not help the catalytic process,[25,77] suggesting that the design of proper catalysts should consider the reductant as well, that is, the added catalysts and the reductant constitute a catalytic system. The reductant oxide could be described as a catalyst support, which could alter the core catalyst morphology as a motif or accommodate the catalyst in the porous structure. Thus, the coordination of the reductant oxide and the core catalyst is important for the design of the catalytic system.

Second, when biomass or organic waste is used as the reductant the reducing efficiency is limited compared to that of metals since it is derived from reductive functional groups; thus, how to increase the reducing efficiency of biomass or organic waste is one obstacle to cope with. As summarized above, the hydroxyl (–OH), aldehyde (–CHO), and amino (NH_2–) groups are the main reductive groups of organic reductants. With the assistance of the hydrothermal environment, the reductive capacity of functional groups can be invoked sufficiently, but the ultimate reducing performance also relies on the chemical structure of the organic reductants. For instance, for carbohydrates, the aldehyde group is the main reductive source, but the exposure of the aldehyde group is difficult to control. Taking glucose as an example, if dehydration or isomerization of glucose happens, the aldehyde group will be consumed or concealed in CO_2 reduction, which will severely compromise the reduction efficiency. Thus, it is urgent to design optimal reaction procedures or catalysts to conserve the reductive functional groups. Yang *et al.*[117] used a two-step reaction strategy to enhance glycolaldehyde production from glucose, as it is a two-carbon aldose that thoroughly cuts off the possibility of dehydration or isomerization reaction, and, therefore, almost two-fold reduction efficiency was achieved compared to the one-step reaction. For biomass using amino groups as the reductive force, such as in microalgae, the dehydration reaction of the amino group with a carboxylic group to form amide is the main reaction consuming amino groups. However, with proper modulation of the solution pH, the dehydration reaction can be sufficiently avoided.[39] Waste plastics such as PVC reduce CO_2 with hydroxyl groups.[101] Although this group can be preserved well under hydrothermal conditions, its reducing capacity is relatively poor compared to those of other functional groups such as aldehyde or amino. Thus, delicately prepared catalysts such as Cu based catalysts are needed to enhance the reducing efficiency.[9] Consequently, to fully utilize the reductive power of functional groups in organic reductants, the general reaction mechanisms should be illustrated clearly with acknowledgment of the possible side reactions that might compromise the functional groups, and optimal reaction procedures, parameters or catalysts must be designed accordingly.

Third, for long-term development, natural biomass is better for use when biomass serves as the reductant. However, natural biomass is very complicated, with not only varied species, but also various chemical compositions (such as carbohydrates, proteins, lipids, lignin, *etc.*). The synergetic effects of these chemical compositions will inevitably affect both the selectivity and the efficiency of CO_2 hydrothermal reduction. Thus, it is necessary to study whether and how the different chemical compositions of biomass will influence CO_2 reduction. Taking the reaction of microalgae with CO_2 as an example, protein was found to be the main reductant, while carbohydrate and lipid reduced less CO_2. In the meantime, reactions between protein and carbohydrate were observed, like the Maillard reaction. However, the reaction between protein and carbohydrate is highly dependent on the solution pH, suggesting it can be partly avoided by proper alkalinity adjustment. On the other hand, it should be noted that the direct use of natural biomass for CO_2 reduction is difficult for achieving high selectivity or efficiency as the compositions of biomass are too complicated. With sufficient acknowledgement of the reaction characteristics of different reductants, certain approaches can be suggested to achieve the target with the basic principle that it is important to

produce active intermediates in the first step and then achieve CO_2 reduction in the second step. Specifically, when carbohydrate is used, cutting the carbon chain to smaller aldoses is one feasible solution to ensure the reducing capacity, which can be accomplished by acid catalyzed pretreatment or the physical process of ball milling. When protein abundant biomass is used, such as microalgae, the hydrolysis of microalgae in the first step is important. After eliminating the products of the Maillard reaction, much higher CO_2 reduction efficiency can be expected with the remaining amino acids. For lignin, it is found that the reactivity is hardly influenced by other chemical compositions, while its degradation pathway is important for the CO_2 reduction and can be modulated by proper catalysts such as Pd or Ru based catalysts.

Fourth, although great progress has been made in the development of hydrothermal CO_2 with renewable reductants, the above analysis suggests that improving the reduction efficiency or producing the target product are still great challenges. Therefore, in-depth understanding of the mechanism of competitive reactions in the hydrothermal environment is desperately needed. The high temperature and high-pressure reaction environment in a sealed reaction box makes it difficult to detect the reaction mechanism. The continuous and rapid development of DFT calculations combined with *in situ* characterization techniques, such as *in situ* synchrotron radiation spectroscopy, NMR, Raman and FTIR spectroscopy and chromatography, will undoubtedly accelerate the progress of understanding the reaction mechanism. On one hand, DFT calculations can be used to deeply reveal the transformative behaviors of the reductants under hydrothermal conditions, which will help to understand the possible catalytic function of hydrothermal water and provide guidance for the design of highly selective catalysts or reaction parameters. On the other hand, advanced *operando* characterization techniques can provide real-time analysis of key intermediates during the reaction, which is conducive to deducing the rate-determining step of the reaction and optimizing the reaction by designing rational procedures such as multi-step reactions. Therefore, the combination of theoretical calculations and advanced *in situ* characterization techniques will help to understand hydrothermal reactions basically and profoundly and thus assist in achieving industrial-level CO_2 hydrothermal reduction with renewable reductants.

Fifth, to meet the requirement of practically implementing CO_2 conversion approaches, the advantages of the summarized methods of hydrothermal CO_2 reduction with renewable reductants include the operable nature of hydrothermal reactions, the storage and transportation convenience of metals or biomass, and the direct use of bicarbonate, the alkaline product after CO_2 capture, as the carbon source. However, the main conundrum to consider is the high temperature and high pressure of hydrothermal reactions. For industrial applications, temperatures around 200 °C can be provided readily, while higher temperatures approaching 300 °C could cause safety issues. Thus, decreasing the temperature of hydrothermal CO_2 reduction to around 200 °C is a necessary consideration. In this aspect, Wang *et al.*[35] achieved CO_2 reduction with methanol at 180 °C with Pd–Cu catalysts, and Ni and Cu were found to decrease the reduction temperature of CO_2 with Fe or Zn as the reductant to around 200 °C. More recently, we found that with Co–Pd catalysts, glucose could reduce CO_2 at around 200 °C as well. These results indicate that, with rationally designed catalysts, the reaction temperature can be reduced sufficiently. By investigating the catalytic mechanism in the above research, the basic thought in designing the target catalyst is to enhance the hydrogenation of CO_2. Thus, normally noble metals such as Pd, Pt, and Ru can be considered as incorporated components in catalysts, and, with the proper added components, the catalytic effect of the core element can be further enhanced. Indeed, our previous research concerning biomass conversion under hydrothermal conditions has inspired a facility for processing organic waste at *ca.* 200 °C with the capacity of 100 kg per day. Thus, a lower reaction temperature approaching 200 °C indicates the possibility of applying the technology practically.

Sixth, for industrial applications, the energy consumption and economic benefit of the process should be considered. For hydrothermal reactions, it is generally acknowledged that water must be heated for the reaction and thus the energy consumption is abundant. As a matter of fact, according to the thermodynamic study of the above summarized research, CO_2 hydrothermal reduction with renewable reductants is always an exothermic process, since the reductants are oxidized as energy donors, which indicates that if the heat preservation of reactors is supplied, once the reaction is started, no more energy is required. More intriguingly, when metals are used as the reductants, the exuded heat of metal oxidation is so large that extra energy might be recovered if the reactors are designed properly. For the financial budget of hydrothermal technology, since special facilities are required for hydrothermal reactions, the expense of the technology is postulated to be large. However, when the oxidation of reductants such as biomass into chemicals or fuels is considered for calculating the economic benefit, the vision might be different. Taking Fe as the reductant for CO_2 conversion as an example, when its recovery is achieved with glycerol reducing Fe_3O_4, it is determined that the economic benefit of one cycle can reach $2.2 for 1 mol CO_2, indicating vast potential in achieving economic benefit from CO_2 hydrothermal reduction. When hydrothermal technology is applied in practice, the up-front investment might be large, but for the long term, the financial benefit is relatively promising due to its fast reaction speed and the feasibility in processing different substrates, as is the case in our facilities for processing organic waste.

Seventh, the most acknowledgeable application of hydrothermal technology is its use in reforming biomass for hydrogen production under supercritical hydrothermal conditions, and recently aqueous phase reforming of biomass under subcritical conditions has been developed, which suggests that hydrogen can first be produced from biomass hydrothermal treatment, and then CO_2 can be hydrogenated in the second step through the process of catalytic hydrogenation. This consideration also aligns with the practical plant built by Li *et al.*,[135,138] where they first use solar energy to achieve electrolysis of water, and then CO_2 is reduced through a thermal

catalytic process. This way, the practical obstacles in harnessing direct CO_2 solar-/electro-reduction can be avoided, and the need for green hydrogen in CO_2 hydrogenation can be achieved. However, when fully considering CO_2 hydrothermal reduction, we assume that direct CO_2 hydrothermal conversion with reductants in a one-pot reaction is superior, with the following advantages: (1) from the macroscopic view, when CO_2 and reductants are present in the same reaction environment, the reductive power and energy held in the reductant can be exploited directly for CO_2 reduction without the need for mass or energy transfer, which can naturally lead to less efficiency lost, and (2) from the mechanistic view, CO_2 hydrothermal reduction rarely follows the pathway of first hydrogen generation and consequent CO_2 hydrogenation. In contrast, it is reduced directly with *in situ* hydrogen from either the hydrogen spillover from the catalyst surface (as in the case with metals as the reductants) or direct hydrogen transfer from the reductant (as in the case with organic reductants), which have proved to be far more efficient than CO_2 hydrogenation. Thus, owing to the improvement in mass and energy transfer under hydrothermal conditions, one-pot CO_2 hydrothermal reduction is postulated to be more efficient.

In summary, although progress is still needed in CO_2 hydrothermal reduction, such as in the broadness of product species, given the improvement in reducing efficiency and stable rational hydrothermal catalysts, the proposed strategy holds promising potential for industrial application due to the native advantages of hydrothermal reactions and the sustainability of the reductants. It is believed that in the foreseeable future, efficient and net carbon benefit CO_2 hydrothermal reduction will make a great breakthrough through systematic mechanistic research and continuous optimization of catalysts and reaction procedures and parameters. Once the concept of hydrothermal CO_2 reduction with renewable reductants can be applied in large-scale industrial application, the global warming and energy crises will be greatly alleviated, and a low-carbon economy can be envisioned.

Author contributions

Zien Tang: conceptualization, methodology, writing – original draft; Xu Liu: data curation, visualization; Yang Yang: software, writing – review & editing, project administration, supervision; Fangming Jin: investigation, resources, validation, supervision.

Conflicts of interest

There are no conflicts to declare.

Acknowledgements

The authors thank the financial support of the National Natural Science Foundation of China (No. 21978170 & 22108171), the Natural Science Foundation of Shanghai (No. 23ZR1435200), and Shanghai Key Laboratory of Hydrogen Science & Center of Hydrogen Science, Shanghai Jiao Tong University, China.

References

1 M. I. Alam, R. Cheula, G. Moroni, L. Nardi and M. Maestri, *Catal. Sci. Technol.*, 2021, **11**, 6601–6629.
2 E. Koohestanian and F. Shahraki, *J. Environ. Chem. Eng.*, 2021, **9**, 105777.
3 N. von der Assen, P. Voll, M. Peters and A. Bardow, *Chem. Soc. Rev.*, 2014, **43**, 7982–7994.
4 T. Kumar and S. Eswari, *Energy Fuels*, 2023, **37**, 3570–3589.
5 H. Salehizadeh, N. Yan and R. Farnood, *Chem. Eng. J.*, 2020, **390**, 124584.
6 S. J. Davis, N. S. Lewis, M. Shaner, S. Aggarwal, D. Arent, I. L. Azevedo, S. M. Benson, T. Bradley, J. Brouwer, Y. M. Chiang, C. T. M. Clack, A. Cohen, S. Doig, J. Edmonds, P. Fennell, C. B. Field, B. Hannegan, B. M. Hodge, M. I. Hoffert, E. Ingersoll, P. Jaramillo, K. S. Lackner, K. J. Mach, M. Mastrandrea, J. Ogden, P. F. Peterson, D. L. Sanchez, D. Sperling, J. Stagner, J. E. Trancik, C. J. Yang and K. Caldeira, *Science*, 2018, **360**, eaas9793.
7 G. Hasrack, M. C. Bacariza, C. Henriques and P. Da Costa, *Catalysts*, 2022, **12**, 36.
8 S. S. Xu, S. Chansai, S. J. Xu, C. E. Stere, Y. L. Jiao, S. H. Yang, C. Hardacre and X. L. Fan, *ACS Catal.*, 2020, **10**, 12828–12840.
9 X. He, M. Liu, Z. Liang, Z. Wang, P. Wang, Y. Liu, H. Cheng, Y. Dai, Z. Zheng and B. Huang, *J. Solid State Chem.*, 2021, **298**, 122113.
10 L. L. Ling, W. Yang, P. Yan, M. Wang and H. L. Jiang, *Angew Chem. Int. Ed. Engl.*, 2022, **61**, e202116396.
11 S. F. Hung, A. Xu, X. Wang, F. Li, S. H. Hsu, Y. Li, J. Wicks, E. G. Cervantes, A. S. Rasouli, Y. C. Li, M. Luo, D. H. Nam, N. Wang, T. Peng, Y. Yan, G. Lee and E. H. Sargent, *Nat. Commun.*, 2022, **13**, 819.
12 J. B. Jiang, A. J. Matula, J. R. Swierk, N. Romano, Y. S. Wu, V. S. Batista, R. H. Crabtree, J. S. Lindsey, H. L. Wang and G. W. Brudvig, *ACS Catal.*, 2018, **8**, 10131–10136.
13 X. Ding, X. Liu, J. Cheng, L. Kong and Y. Guo, *Catal. Sci. Technol.*, 2022, **12**, 4740–4752.
14 S. Wang, A. A. Tountas, W. Pan, J. Zhao, L. He, W. Sun, D. Yang and G. A. Ozin, *Small*, 2021, **17**, e2007025.
15 N. Dhabarde, J. Selvaraj, A. Yuda, A. Kumar and V. R. Subramanian, *Int. J. Hydrogen Energy*, 2022, **47**, 30908–30936.
16 S. Pan, J. Li, Z. Wen, R. Lu, Q. Zhang, H. Jin, L. Zhang, Y. Chen and S. Wang, *Adv. Energy Mater.*, 2021, **12**, 2004002.
17 Z. H. Liu, K. Wang, Y. Chen, T. W. Tan and J. Nielsen, *Nat. Catal.*, 2020, **3**, 274–288.
18 C. Hepburn, E. Adlen, J. Beddington, E. A. Carter, S. Fuss, N. Mac Dowell, J. C. Minx, P. Smith and C. K. Williams, *Nature*, 2019, **575**, 87–97.
19 E. L. Kunkes, D. A. Simonetti, R. M. West, J. C. Serrano-Ruiz, C. A. Gartner and J. A. Dumesic, *Science*, 2008, **322**, 417–421.
20 O. Faye, J. Szpunar and U. Eduok, *Int. J. Hydrogen Energy*, 2022, **47**, 13771–13802.

21 T. M. McCollom and J. S. Seewald, *Chem. Rev.*, 2007, **107**, 382–401.
22 W. Martin, J. Baross, D. Kelley and M. J. Russell, *Nat. Rev. Microbiol.*, 2008, **6**, 805–814.
23 G. Proskurowski, M. D. Lilley, J. S. Seewald, G. L. Fruh-Green, E. J. Olson, J. E. Lupton, S. P. Sylva and D. S. Kelley, *Science*, 2008, **319**, 604–607.
24 S. Navarro-Jaen, M. Virginie, J. Bonin, M. Robert, R. Wojcieszak and A. Y. Khodakov, *Nat. Rev. Chem*, 2021, **5**, 564–579.
25 D. He, X. Wang, Y. Yang, R. He, H. Zhong, Y. Wang, B. Han and F. Jin, *Proc. Natl. Acad. Sci. U. S. A.*, 2021, **118**, e2115059118.
26 R. He, B. Hu, H. Zhong, F. Jin, J. Fan, Y. H. Hu and Z. Jing, *Chem. Commun.*, 2019, **55**, 1056–1059.
27 B. Y. Hu, Z. Z. Jing, J. J. Fan, G. D. Yao and F. M. Jin, *Catal. Today*, 2016, **263**, 128–135.
28 Z. B. Huo, M. B. Hu, X. Zeng, J. Yun and F. M. Jin, *Catal. Today*, 2012, **194**, 25–29.
29 C. L. Jiang, H. Zhong, G. D. Yao, J. Duo and F. M. Jin, *Int. J. Hydrogen Energy*, 2017, **42**, 17476–17487.
30 X. Liu, H. Zhong, C. Wang, D. He and F. Jin, *Energy Sci. Eng.*, 2022, **10**, 1601–1613.
31 Z. Ni, H. Zhong, Y. Yang, G. Yao, B. Jin and F. Jin, *ACS Sustainable Chem. Eng.*, 2019, **7**, 5827–5834.
32 Z. Shen, Y. Zhang and F. Jin, *RSC Adv.*, 2012, **2**, 797–801.
33 X. Wang, Y. Yang, T. Wang, H. Zhong, J. Cheng and F. Jin, *ACS Sustainable Chem. Eng.*, 2021, **9**, 1203–1212.
34 X. G. Wang, Y. Yang, H. Zhong, R. T. He, J. Cheng and F. M. Jin, *Catal. Today*, 2020, **350**, 136–141.
35 X. G. Wang, Y. Yang, H. Zhong, T. F. Wang, J. Cheng and F. M. Jin, *Green Chem.*, 2021, **23**, 430–439.
36 Y. Q. Wang, F. M. Jin, M. Sasaki, Wahyudiono, F. W. Wang, Z. Z. Jing and M. Goto, *AIChE J.*, 2013, **59**, 2096–2104.
37 Y. Q. Wang, F. M. Jin, X. Zeng, G. D. Yao and Z. Z. Jing, *Int. J. Hydrogen Energy*, 2013, **38**, 760–768.
38 L. X. Wu, Y. Yang, J. Cheng, X. G. Wang, Q. Huang and F. M. Jin, *React. Chem. Eng.*, 2022, **7**, 839–843.
39 Y. Yang, H. Zhong, R. He, X. Wang, J. Cheng, G. Yao and F. Jin, *Green Chem.*, 2019, **21**, 1247–1252.
40 Y. Yang, H. Zhong, G. Yao, R. He, B. Jin and F. Jin, *Catal. Today*, 2018, **318**, 10–14.
41 G. Yao, F. Chen, Z. Huo and F. Jin, *Int. J. Hydrogen Energy*, 2016, **41**, 9135–9139.
42 G. Yao, J. Duo, B. Jin, H. Zhong, L. Lyu, Z. Ma and F. Jin, *J. Energy Chem.*, 2017, **26**, 881–890.
43 G. Yao, X. Zeng, Y. Jin, H. Zhong, J. Duo and F. Jin, *Int. J. Hydrogen Energy*, 2015, **40**, 14284–14289.
44 X. Zeng, M. Hatakeyama, K. Ogata, J. Liu, Y. Wang, Q. Gao, K. Fujii, M. Fujihira, F. Jin and S. Nakamura, *Phys. Chem. Chem. Phys.*, 2014, **16**, 19836–19840.
45 X. Zeng, F. M. Jin, Z. B. Huo, T. Mogi, A. Kishita and H. Enomoto, *Energy Fuels*, 2011, **25**, 2749–2752.
46 X. Zeng, F. Jin, G. Yao and Z. Huo, *Int. J. Hydrogen Energy*, 2016, **41**, 9140–9144.
47 S. Zhang, Z. B. Huo, D. Z. Ren, J. Luo, J. Fu, L. Li and F. M. Jin, *Chin. J. Chem. Eng.*, 2016, **24**, 126–131.
48 H. Zhong, Y. Gao, G. D. Yao, X. Zeng, Q. J. Li, Z. B. Huo and F. M. Jin, *Chem. Eng. J.*, 2015, **280**, 215–221.
49 H. Zhong, L. Ma, Y. Y. Zhu, B. B. Jin, T. F. Wang, Y. G. Wang and F. M. Jin, *J. Supercrit. Fluids*, 2020, **157**, 104717.
50 H. Zhong, H. S. Yao, J. Duo, G. D. Yao and F. M. Jin, *Catal. Today*, 2016, **274**, 28–34.
51 Y. J. Zhu, Y. Yang, X. G. Wang, H. Zhong and F. M. Jin, *Energy Sci. Eng.*, 2019, **7**, 881–889.
52 J. Duo, F. Jin, Y. Wang, H. Zhong, L. Lyu, G. Yao and Z. Huo, *Chem. Commun.*, 2016, **52**, 3316–3319.
53 C. He, G. Tian, Z. Liu and S. Feng, *Org. Lett.*, 2010, **12**, 649–651.
54 F. M. Jin, Y. Gao, Y. J. Jin, Y. L. Zhang, J. L. Cao, Z. Wei and R. L. Smith, *Energy Environ. Sci.*, 2011, **4**, 881–884.
55 B. Wu, Y. Gao, F. M. Jin, J. L. Cao, Y. X. Du and Y. L. Zhang, *Catal. Today*, 2009, **148**, 405–410.
56 A. Steinfeld, *Int. J. Hydrogen Energy*, 2002, **27**, 611–619.
57 N. J. Pester, K. Ding and W. E. Seyfried, *Geology*, 2014, **42**, 255–258.
58 X. Liu, Y. Guo, D. H. Xu and Q. Q. Guan, *J. Cleaner Prod.*, 2022, **366**, 132978.
59 X. Liu, Y. Guo, A. Dasgupta, H. He, D. Xu and Q. Guan, *Renewable Energy*, 2022, **183**, 627–650.
60 A. A. Peterson, F. Vogel, R. P. Lachance, M. Fröling, M. J. Antal and J. W. Tester, *Energy Environ. Sci.*, 2008, **1**, 32–65.
61 M. Akizuki, T. Fujii, R. Hayashi and Y. Oshima, *J. Biosci. Bioeng.*, 2014, **117**, 10–18.
62 S. S. Toor, L. Rosendahl and A. Rudolf, *Energy*, 2011, **36**, 2328–2342.
63 V. Lehr, M. Sarlea, L. Ott and H. Vogel, *Catal. Today*, 2007, **121**, 121–129.
64 N. H. Sleep, *Origins Life Evol. Biospheres*, 1986, **16**, 179–180.
65 B. Herschy, A. Whicher, E. Camprubi, C. Watson, L. Dartnell, J. Ward, J. R. Evans and N. Lane, *J. Mol. Evol.*, 2014, **79**, 213–227.
66 V. Sojo, B. Herschy, A. Whicher, E. Camprubi and N. Lane, *Astrobiology*, 2016, **16**, 181–197.
67 J. Fiebig, A. B. Woodland, J. Spangenberg and W. Oschmann, *Geochim. Cosmochim. Acta*, 2007, **71**, 3028–3039.
68 A. D. Aubrey, H. J. Cleaves and J. L. Bada, *Origins Life Evol. Biospheres*, 2009, **39**, 91–108.
69 Y. Q. Chen, Z. Z. Jing, J. J. Miao, Y. Zhang and J. J. Fan, *Int. J. Hydrogen Energy*, 2016, **41**, 9123–9127.
70 H. Takahashi, T. Kori, T. Onoki, K. Tohji and N. Yamasaki, *J. Mater. Sci.*, 2007, **43**, 2487–2491.
71 G. Tian, C. He, Y. Chen, H. M. Yuan, Z. W. Liu, Z. Shi and S. H. Feng, *ChemSusChem*, 2010, **3**, 323–324.
72 G. Tian, H. Yuan, Y. Mu, C. He and S. Feng, *Org. Lett.*, 2007, **9**, 2019–2021.
73 X. Zeng, G. D. Yin, Y. Y. Zhou and J. F. Zhao, *Molecules*, 2022, **27**, 7371.
74 B. Jin, L. Luo and L. Xie, *ACS Omega*, 2021, **6**, 11280–11285.
75 H. W. Suh, T. J. Schmeier, N. Hazari, R. A. Kemp and M. K. Takase, *Organometallics*, 2012, **31**, 8225–8236.

76 F. Jin, X. Zeng, J. Liu, Y. Jin, L. Wang, H. Zhong, G. Yao and Z. Huo, *Sci. Rep.*, 2014, **4**, 4503.
77 Y. Le, H. Zhong, Y. Yang, R. T. He, G. D. Yao and F. M. Jin, *J. Energy Chem.*, 2017, **26**, 936–941.
78 L. Y. Wang, G. D. Yao, Z. Z. Jing and F. M. Jin, *Adv. Mater. Res.*, 2014, **1073–1076**, 39–42.
79 H. Zhong, L. Wang, Y. Yang, R. He, Z. Jing and F. Jin, *ACS Appl. Mater. Interfaces*, 2019, **11**, 42149–42155.
80 J. Liu, X. Zeng, M. Cheng, J. Yun, Q. Li, Z. Jing and F. Jin, *Bioresour. Technol.*, 2012, **114**, 658–662.
81 Z. Shen, Y. L. Zhang and F. M. Jin, *Green Chem.*, 2011, **13**, 820–823.
82 Y. Q. Wang, F. W. Wang, C. J. Li and F. M. Jin, *Int. J. Hydrogen Energy*, 2016, **41**, 9128–9134.
83 A. Costine, J. S. C. Loh, F. Busetti, C. A. Joll and A. Heitz, *Ind. Eng. Chem. Res.*, 2013, **52**, 5572–5581.
84 C. A. Ramírez-López, J. R. Ochoa-Gómez, S. Gil-Río, O. Gómez-Jiménez-Aberasturi and J. Torrecilla-Soria, *J. Chem. Technol. Biotechnol.*, 2011, **86**, 867–874.
85 H. Kishida, F. Jin, X. Yan, T. Moriya and H. Enomoto, *Carbohydr. Res.*, 2006, **341**, 2619–2623.
86 Z. Shen, M. Y. Gu, M. Zhang, W. J. Sang, X. F. Zhou, Y. L. Zhang and F. M. Jin, *RSC Adv.*, 2014, **4**, 15256–15263.
87 W. B. Yan, B. B. Jin, J. Cheng, X. Y. Shi, H. Zhong and F. M. Jin, *ACS Sustainable Chem. Eng.*, 2022, **10**, 5374–5383.
88 J. Su, L. Yang, X. Yang, M. Lu, B. Luo and H. Lin, *ACS Sustainable Chem. Eng.*, 2014, **3**, 195–203.
89 J. Park, A. H. Valekar, K. R. Oh, A. Awad, I. H. Song, C. Yoo, J. J. An and Y. K. Hwang, *Chem. Eng. J.*, 2023, **463**, 142410.
90 Y. Yang, H. Zhong, J. Cheng, Y. H. Hu, R. L. Smith and F. Jin, *Next Energy*, 2023, **1**, 100037.
91 M. Andérez-Fernández, E. Pérez, A. Martín and M. D. Bermejo, *J. Supercrit. Fluids*, 2018, **133**, 658–664.
92 M. Andérez-Fernández, S. Ferrero, J. P. S. Queiroz, E. Pérez, C. M. Álvarez, Á. Martín and M. D. Bermejo, *J. Taiwan Inst. Chem. Eng.*, 2022, **139**, 104504.
93 M. Andérez-Fernández, E. Pérez, S. Ferrero, C. M. Álvarez, J. Gumiel, Á. Martín and M. D. Bermejo, *Chem. Eng. J.*, 2023, **453**, 139741.
94 K. R. Oh, A. H. Valekar, G. Y. Cha, M. Lee, C. Yoo and Y. K. Hwang, *J. CO2 Util.*, 2022, **60**, 101981.
95 G. Ding, J. Su, C. Zhang, K. Tang, L. Yang and H. Lin, *ChemSusChem*, 2018, **11**, 2029–2034.
96 J. C. Li, P. D. Zhu, H. Zhong, Y. Yang, J. Cheng, Y. G. Wang and F. M. Jin, *ACS Sustainable Chem. Eng.*, 2021, **9**, 4791–4800.
97 E. Smidt and K. Meissl, *Waste Management*, 2007, **27**, 268–276.
98 M. Anderez-Fernandez, E. Perez, A. Martin, J. McGregor and M. D. Bermejo, *ACS Sustainable Chem. Eng.*, 2022, **10**, 16948–16957.
99 K. Ragaert, L. Delva and K. Van Geem, *Waste Management*, 2017, **69**, 24–58.
100 C. Jehanno, J. W. Alty, M. Roosen, S. De Meester, A. P. Dove, E. Y. Chen, F. A. Leibfarth and H. Sardon, *Nature*, 2022, **603**, 803–814.
101 J. Wang, X. Li, M. Wang, T. Zhang, X. Chai, J. Lu, T. Wang, Y. Zhao and D. Ma, *ACS Catal.*, 2022, **12**, 6722–6728.
102 Y. Li, M. Wang, X. Liu, C. Hu, D. Xiao and D. Ma, *Angew Chem. Int. Ed. Engl.*, 2022, **61**, e202117205.
103 X. Liang, M. Wang and D. Ma, *J. Am. Chem. Soc.*, 2024, **146**, 2711–2717.
104 W. J. Chen, Y. C. Jiao, Y. Liu, M. Wang, F. Zhang and D. Ma, *CCS Chem.*, 2023, 1–8.
105 L. H. Lu, H. Zhong, T. F. Wang, J. N. Wu, F. M. Jin and T. Yoshioka, *Green Chem.*, 2020, **22**, 352–358.
106 Y. Zhuge, G. Fan, Y. Lin, L. Yang and F. Li, *Dalton Trans.*, 2019, **48**, 9161–9172.
107 L. Lin, X. He, X. G. Zhang, W. Ma, B. Zhang, D. Wei, S. Xie, Q. Zhang, X. Yi and Y. Wang, *Angew. Chem.*, 2022, **135**, e202214959.
108 Z. Liu, E. Huang, I. Orozco, W. Liao, R. M. Palomino, N. Rui, T. Duchon, S. Nemsak, D. C. Grinter, M. Mahapatra, P. Liu, J. A. Rodriguez and S. D. Senanayake, *Science*, 2020, **368**, 513–517.
109 Y. Zhu, Y. Yang, X. Wang, H. Zhong and F. Jin, *Energy Sci. Eng.*, 2019, **7**, 881–889.
110 S. Saedy, M. A. Newton, M. Zabilskiy, J. H. Lee, F. Krumeich, M. Ranocchiari and J. A. van Bokhoven, *Catal. Sci. Technol.*, 2022, **12**, 2703–2716.
111 L. Y. Lyu, F. M. Jin, H. Zhong, H. J. Chen and G. D. Yao, *RSC Adv.*, 2015, **5**, 31450–31453.
112 Y. Le, G. D. Yao, H. Zhong, B. B. Jin, R. T. He and F. M. Jin, *Catal. Today*, 2017, **298**, 124–129.
113 J. Q. Zhao, Q. Yang, R. Shi, G. I. N. Waterhouse, X. Zhang, L. Z. Wu, C. H. Tung and T. R. Zhang, *NPG Asia Mater.*, 2020, **12**, 5.
114 L. Wang, Y. Dong, T. Yan, Z. Hu, F. M. Ali, D. M. Meira, P. N. Duchesne, J. Y. Y. Loh, C. Qiu, E. E. Storey, Y. Xu, W. Sun, M. Ghoussoub, N. P. Kherani, A. S. Helmy and G. A. Ozin, *Nat. Commun.*, 2020, **11**, 2432.
115 S. B. Ning, H. Xu, Y. H. Qi, L. Z. Song, Q. Q. Zhang, S. X. Ouyang and J. H. Ye, *ACS Catal.*, 2020, **10**, 4726–4736.
116 D. Mateo, J. Albero and H. García, *Appl. Catal., B*, 2018, **224**, 563–571.
117 Y. H. Pei, W. Gu, S. Cheng, S. H. Xiao, C. L. Wang, Y. Yang, H. Zhong and F. M. Jin, *ACS Catal.*, 2023, **13**, 12082–12091.
118 J. Su, L. Yang, M. Lu and H. Lin, *ChemSusChem*, 2015, **8**, 813–816.
119 Q. Y. Bi, J. D. Lin, Y. M. Liu, X. L. Du, J. Q. Wang, H. Y. He and Y. Cao, *Angew Chem. Int. Ed. Engl.*, 2014, **53**, 13583–13587.
120 L. G. Lundsted, *J. Am. Chem. Soc.*, 1949, **71**, 323.
121 G. Bredig and S. R. Carter, *Ber. Dtsch. Chem. Ges.*, 2006, **47**, 541–545.
122 T. Mandal, A. Kumar, J. Panda, T. Kumar Dutta and J. Choudhury, *Angew Chem. Int. Ed. Engl.*, 2023, **62**, e202314451.
123 S. Wang, S. Hou, C. Wu, Y. Zhao and X. Ma, *Chin. Chem. Lett.*, 2019, **30**, 398–402.
124 Y. Shen, Q. Zheng, Z. N. Chen, D. Wen, J. H. Clark, X. Xu and T. Tu, *Angew Chem. Int. Ed. Engl.*, 2021, **60**, 4125–4132.

125 S. Mukhopadhyay, M. S. Naeem, G. Shiva Shanker, A. Ghatak, A. R. Kottaichamy, R. Shimoni, L. Avram, I. Liberman, R. Balilty, R. Ifraemov, I. Rozenberg, M. Shalom, N. Lopez and I. Hod, *Nat. Commun.*, 2024, **15**, 3397.
126 Z. Wang, H. Li, T. Dong, Y. Geng, X. Tian, R. Chang, J. Lai, S. Feng and L. Wang, *Chem. Eng. J.*, 2024, **489**, 151238.
127 N. Thonemann and A. Schulte, *Environ. Sci. Technol.*, 2019, **53**, 12320–12329.
128 L. Ai, S. F. Ng and W. J. Ong, *ChemSusChem*, 2022, **15**, e202200857.
129 R. Aldaco, I. Butnar, M. Margallo, J. Laso, M. Rumayor, A. Dominguez-Ramos, A. Irabien and P. E. Dodds, *Sci. Total Environ.*, 2019, **663**, 738–753.
130 S. Kibria Nabil, S. McCoy and M. G. Kibria, *Green Chem.*, 2021, **23**, 867–880.
131 H. H. Khoo, I. Halim and A. D. Handoko, *J. CO2 Util.*, 2020, **41**, 101229.
132 J. Q. Wang, X. J. Liu, J. J. Ma, S. Zhang, H. R. Liu, Y. L. Dong and Q. Y. Yang, *Green Chem. Eng.*, 2023, DOI: **10.1016/j.gce.2023.10.003**.
133 G. Z. S. Ling, J. J. Foo, X. Q. Tan and W. J. Ong, *ACS Sustainable Chem. Eng.*, 2023, **11**, 5547–5558.
134 G. Zang, P. Sun, A. Elgowainy and M. Wang, *Environ. Sci. Technol.*, 2021, **55**, 5248–5257.
135 Y. Khojasteh-Salkuyeh, O. Ashrafi, E. Mostafavi and P. Navarri, *J. CO2 Util.*, 2021, **50**, 101608.
136 J. Xu, J. Cheng, R. T. He, J. Q. Lu, C. L. Wang, H. Zhong and F. M. Jin, *Front. Environ. Sci. Eng.*, 2023, **17**, 127.
137 K. Lee, H. Yan, Q. M. Sun, Z. H. Zhang and N. Yan, *Acc. Mater. Res.*, 2023, **4**, 746–757.
138 H. Luo, J. Barrio, N. Sunny, A. Li, L. Steier, N. I. Shah, I. E. L. Stephens and M. M. Titirici, *Adv. Energy Mater.*, 2021, **11**, 2101180.